EVALUATION OF CORROSION PROPERTIES FOR USE OF AZ31B IN BIOABSORBABLE STENTS AND IN VIVO CORROSION RATE PREDICTION USING FEA

Jared Vidales, Austin Schader, Jenna Jerman, Michael Turovskiy
Materials Engineering Department
California Polytechnic State University
Advisor: Dr. Trevor Harding

June 4, 2012

Approval Page

Project Title: EVALUATION OF CORROSION PROPERTIES FOR USE of AZ31B IN BIOABSORBABLE STENTS AND IN VIVO CORROSION RATE PREDICTION USING FEA

Author: Jared Vidales,
Austin Schader
Jenna Jerman
Michael Turovskiy

Date Submitted: June 4, 2012

CAL POLY STATE UNIVERSITY

Materials Engineering Department

Since this project is a result of a class assignment, it has been graded and accepted as fulfillment of the course requirements. Acceptance does not imply technical accuracy or reliability. Any use of the information in this report, including numerical data, is done at the risk of the user. These risks may include catastrophic failure of the device or infringement of patent or copyright laws. The students, faculty, and staff of Cal Poly State University, San Luis Obispo cannot be held liable for any misuse of the project.

Prof. Trevor Harding
Faculty Advisor

_____
Signature

Prof. Trevor Harding
Department Chair

_____
Signature

Table of Contents

List of Figures

List of Tables

Abstract

Evaluation of Corrosion Properties for use of AZ31B Stents and In Vivo Corrosion Rate Prediction using FEA

By: Jared Vidales, Austin Schader, Jenna Jerman, Michael Turovskiy

AZ31B was heat treated to evoke more controlled and uniform corrosion. 1/16" diameter AZ31B wire was cut into six samples each 1" long. The samples underwent heat treatments following ASTM B661-06. Samples were weighed and placed into three different in vitro environments. In the first scenario two samples of each heat treatment were individually placed in 50 ml of saline solution at 0.9% sodium, in a static test tube at 37°C temperature. Two samples were placed in 100 ml of 0.9% saline solution in a 250 ml stirring beaker with an average whirlpool depth of 1". Two of each sample was placed into 50 ml of saline solution at 0.9% sodium at room temperature. The final experiment placed an air cooled sample in 0.9% saline solution in a 6mm tube with a flow rate of 325ml/min at 37°C. All samples were removed at a 3 day, dried, and weighed. Mass loss was recorded, and samples were returned to solution. Samples ranged from 32% mass loss in quenched samples to 17% mass loss in the control samples (as manufactured) over fifteen days. All samples failed as possible stent candidate materials do to the unpredictability of their corrosion in both rate and uniformity. Experimental data was used to create a theoretical mathematic model and COMSOL FEA model that synthesized experimental data and physiological effects such as wall shear stress to predict the corrosion rate for future testing as well as stent geometry optimization to promote vascular health and limit the restenosis event.

Keywords: Stent, Corrosion, Heat Treatment, Microstructure, Shear Stress, Geometry, Saline , NaCl, FEA Model, COMSOL, Dynamic Testing, Static Testing.

Chapter 1: Introduction

1.1 Motivation for Stent Technology

Heart disease is the leading cause of death in the United States, and accounts for almost 25% of deaths each year. Atherosclerosis is a common type of heart disease that often results in angioplasty and stent implantation. Atherosclerosis is plaque formation and the hardening of a vessel that can occur due to smoking, obesity, inactivity, high plasma cholesterol, and variable hemodynamics. Stent endoprotheses (Figure 1) are often used to treat cardiovascular disease due to the high success rate, long-term effectiveness in restoring the lumen and flow conditions, decreased medical expense per patient, and the shorter recovery time.

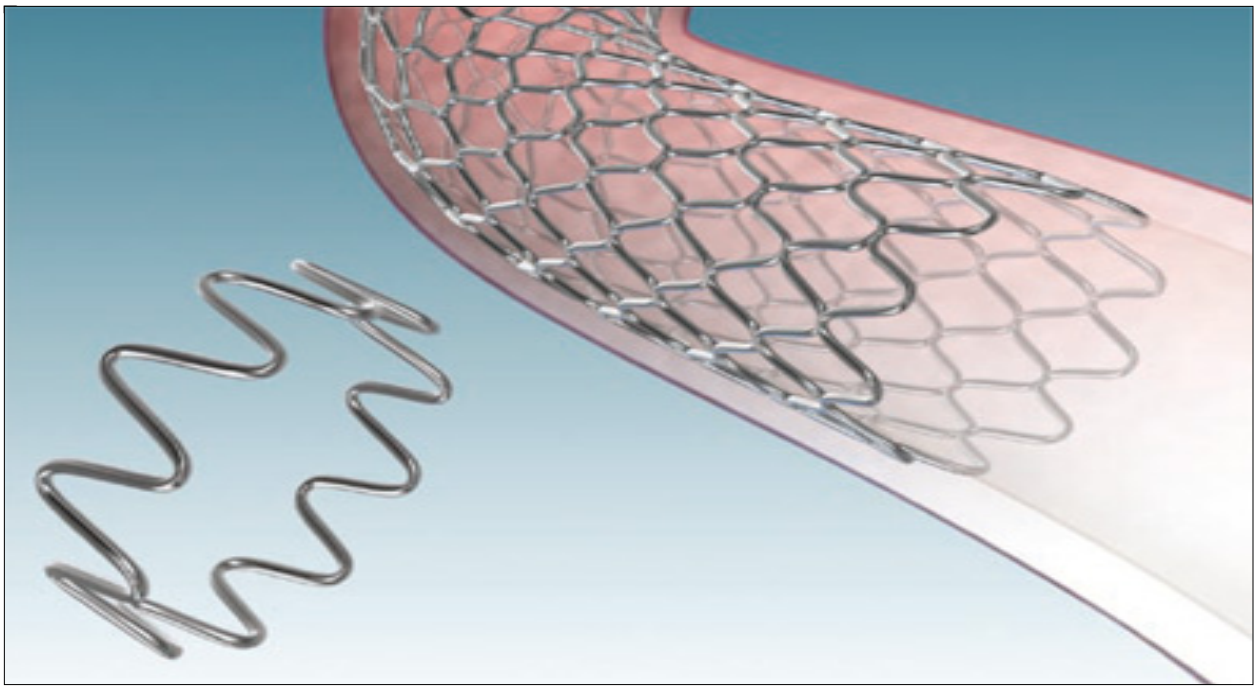

FIGURE 1: THROUGH BALLOON ANGIOPLASTY STENTS REOPEN THE ARTERY TO ALLOW BLOOD TO CONTINUE TO FLOW. (WWW.MEDTRONICSTENTS.COM)

Stents restore blood perfusion through the vessel to necessary tissues, but there exists approximately a 20%-30% chance of a restenosis event within the first six months following the implantation procedure [1]. Restenosis is largely due to excessive cell proliferation and thrombosis, or blood clots resulting from damage to the vasculature during expansion of the stent. Restenosis decreases in the lumen diameter, limiting blood flow through the vessel.

Thrombosis is addressed through the administration of anti-platelet drugs. Excessive cell proliferation can be prevented with the use of drug eluting stents (DES). DES are stents coated with drugs that are slowly released to inhibit cell growth. A disadvantage to DES is they are coated with nonspecific anti-proliferative drugs that prevent all cell growth. Following stenting it is desirable for endothelial cells to grow and coat the metallic structure. However, smooth muscles cells also can grow, which can increase the probability of restenosis. DES coatings and drugs are not limited to controlling an abundance of smooth muscle cells, but also endothelial cells. Endothelial cells naturally emit signals to regulate smooth muscle cells, and, if allowed to grow, decrease the possibility of thrombogenicity and promote vascular healing.

Additional limitations to current stents include: vessel irritation of endothelial cells, possible immune reaction and inflammation due to persistent metallic presence in the vessel, and mismatches in mechanical behavior within the vasculature. Mismatches occur because the stent structure impairs the lumen geometry by limiting vessel expansion. Stents provide limitations such as restenosis, due to cell proliferation and thrombogenicity; these events are issues that arise due to the stent being a permanent structure.

Beyond the time required to allow for healing of the vessel, stents are unnecessary and provide no advantage. Their prolonged presence can contribute to an increase in thrombosis and cell proliferation. A possible solution to these limitations may be the use of biodegradable stents to limit the medical issues that permanent metal stents promote. For these reasons, current research focuses on biodegradable stents, which dissolve in the biological environment after a controlled time period, allowing for vessel recovery and growth, while limiting harmful factors of permanent stents. Biodegradable stents offer more physiological repair, better reconstruction of the damaged vessel site, and allow for appropriate tissue growth. Controlled degradation of the material allows for greater vessel remodeling, decreases the event of late stent thrombosis, because the stent is no longer present, allows for restoration of vasomotion, and facilitates repeated treatments to the area. Therefore, it is the aim of this project to discuss and explore the possibility of degrading metallic stents, to limit the negative effects of permanent metallic stents.

1.2 Sponsor Background and Needs

Medtronic is a biotech company whose goal is to determine if magnesium and its alloys are suitable as a material for degradable stents. Their need is for background research and initial testing to determine if it is feasible to pursue metallic alloys as a possible solution for bioabsorbable stents. The project scope was outlined by Medtronic to include the following parameters and guidelines:

1. Identify bench tests to characterize the degradation behaviors of magnesium-based alloys. Rates, uniformity, and reproducibility must be considered.
2. Identify options to control corrosion rates.
3. Incorporate the impact of the loading conditions on the material.

1.3 Formal Project Definition and Objectives

Approximately six months are required for the stent to counteract the negative remodeling to limit restenosis. Most patients experience lumen enlargement following this initial period, making the stent unnecessary following the first six months. Current magnesium alloys are absorbed in days or weeks, which is too short to prevent constrictive remodeling and restenosis []. Numerous studies investigate and characterize the corrosive behavior of magnesium alloys in artificial physiological fluids, which reaffirms that magnesium corrodes too rapidly due to the higher pH and ion concentrations present in vivo []. Therefore, the tissues have insufficient time to heal before the stent degrades. Without the stent lasting for approximately six months, the prevention of constrictive remodeling is limited and does not provide adequate time for provide the benefits a stent provides.

Ideally bioabsorbable stents will corrode in a uniform linear relationship (Figure 2.). The aim of our project is to meet all of Medtronic's goals, as outlined above, and to try to identify options to more closely model ideal bioabsorbable behavior in magnesium based stents.

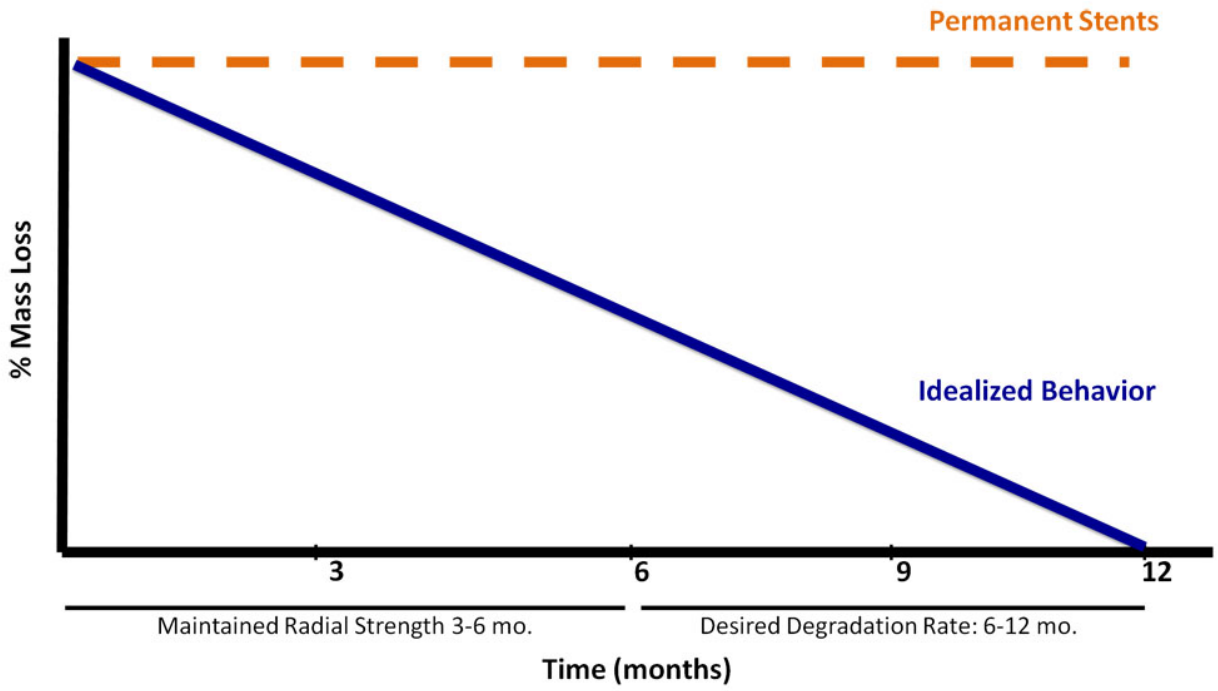

FIGURE 2: IDEAL BIOABSORBABLE STENT BEHAVIOR VS. PERMANENT STENT BEHAVIOR. BY EXHIBITING A LINEAR absorption rate a stent can easily be controlled and monitored for ideal behavior.

1.4 Existing Technologies and Products

1.4.1 Testing Technologies

Common testing techniques for characterizing the corrosion rates of different magnesium alloys include immersion tests and electrochemical tests. These testing types are quick, less complicated than alternative testing techniques, and inexpensive. However, it is difficult to extrapolate the results of the test to predict the system lifetime. Complexities in characterizing corrosion arise that make corrosion rates not directly comparable and produce different local corrosion patterns: anatomical position, different mechanical loading situation, variant pH and ion concentrations, and variations in local blood flow and fluid content. In vivo animal testing shows in vitro and in vivo corrosion rates are not significantly related. On average, rates determined from in vivo tests are approximately four orders of magnitude smaller than those from in vitro testing. Data produced in vitro are not closely correlated to data obtained in vivo due to variations in blood component content and simulated body fluid (SBF) used in testing, and the composition of the corrosive medium influence corrosion behavior [13]. For example, the presence or absence of the proteins can alter the formation of a corrosion-blocking layer on the magnesium alloy, promoting or inhibiting corrosion protection. Flow of the medium has a significant

effect on corrosion rate, so static immersion testing is not effective in determining a relation between in vitro and in vivo conditions that affect degradation. Therefore, in vitro tests for corrosion cannot be used to predict corrosion rates of magnesium in vivo [13].

1.4.2 Stent Products

The first bioabsorbable stent implanted in humans was designed by Biotronik, and was a balloon-expandable magnesium alloy WE-43. The Clinical Performance and Angiographic Results of Coronary Stenting with Absorbable Metal Stents wass a trial study that provided 63 patients with the implant. The arterial wall coverage of the stent and radial strength at implantation was similar to conventional stainless steel stents. Absorption occured via surface erosion, and the thickness of the struts is decreased as the stent was absorbed. The results of the trial were: the stent was successfully deployed but sufficient radial support was lost within days and the stent absorbed within two months, providing insufficient radial strength to counteract the forces experienced due to negative remodeling. Additionally, an anti-proliferating drug was not administered, and the event of restenosis within the first four months was approximately 50%. Future designs require prolonged period of radial support and potentially coating the stent with drugs to limit cell proliferation [10].

Abbott Vascular produced the first bioabsorbable stent with outcomes similar to DES with a time period of two years, called the BVS everolimus-eluting stent. The stent configuration was a backbone of PLLA polymer with a poly-D,L-lactide polymer coating. The coating time-releases the drug everolimus, and stent absorption occurs via bulk erosion. This technology built off previous BVS stent designs, but the polymer was processed differently to provide greater radial strength for a longer duration up to many months, while maintaining the two year absorption rate. This design, in comparison to the Biotronik design, covered more vessel area (approx. 25%), which provides more uniform vessel wall support and uniform drug delivery. A trial study showed great success of stent deployment in 30 patients, with successful delivery of the BVS device in 94% of patients. There was a 16.8% reduction in luminal area due to cell proliferation, and additional shrinkage of the stent area of 12%. Despite the stent shrinkage, the stent performed mechanical functions required to resist negative remodeling, limiting restenosis, and delivery of anti-proliferative drugs limited excess cell growth [10].

Chapter 2: Design Development

2.1 Biological Performance

A material is classified as biocompatible based on the materials ability to perform with an appropriate host response in a specific application [15]. Therefore we must consider both the material properties and the biological reaction to ensure that the chosen material is appropriate for the given application.

The following variables have been identified, but not limited to the importance of overall biocompatibility of a biomaterial: alloys present, geometry, degradation characteristics, surface chemistry, bulk material chemistry and mechanical properties. Therefore, alteration of these characteristics through fabrication or processing techniques is critical to produce an implant with maximal biocompatibility.

2.2 Biological Environment and Degradation

Biodegradation can occur in an uncontrolled manner. This leads to structural breakdown of the material and premature failure of the device. Although the body provides a relatively mild environment with a neutral pH and constant temperature, the presence of aqueous media containing ions facilitates the corrosion of metallic implants [12]. Also specific reactions, such as the actions of inflammatory cells, can change the local chemistry around the device directly after implantation. These inflammatory cells may attach to the biomaterial surface and excrete strong oxidizing agents, such as peroxides, as well as lower the pH drastically in the area, which can further encourage degradation of the material [12].

The biological response is highly affected by the proteins that adsorb to its surface. Therefore controlling protein adsorption to the biomaterial surfaces is a key aspect to assuring biocompatibility. The protein and cellular response to the material determines the overall success of a biomaterial.

Chapter 3: Materials and Methodology

3.1 Alloy Selection

Magnesium alloys in the AZxx series are currently being explored for numerous possible bioabsorbable applications within the body. The AZxx series contains primarily magnesium and aluminum (0-10%) as well as trace amounts of other elements such as zinc. The most corrosion resistant of this series is AZ91E; however, AZ91E (9-10% Al) was not readily available at the time of experimentation thus AZ31B (2.5-3.5% Al) was used as a replacement. AZ91E would have been the ideal candidate as it provides the maximum dissolved Al within the Mg matrix, which inhibits corrosion. AZ91E is also capable of undergoing aging to form coherent fine precipitates of Al that limit corrosion. AZ31B does not have the minimum amount of dissolved aluminum to supersaturate and form precipitates following aging.

3.2 Corrosion of Magnesium

Magnesium corrosion within an in vivo environment is complex. In order to be used as a stent, AZ31B has several stages of corrosion that must be characterized. First, as-cast AZ31B undergoes the growth of passive Mg oxide films instantly when exposed to an oxygen rich environment. The thickness of the oxide film and varies with the oxygen content as well as other elemental content the Mg is exposed to in processing governed by diffusion. Second, when the stent is placed into the in vivo environment the Mg can undergo galvanic corrosion, intergranular corrosion, or intragranular corrosion. Corrosion types occur simultaneously or independently. Galvanic corrosion is corrosion between areas of different chemical potentials, and can occur due to imperfections in the distribution of the phases within the alloy (Mg, Al, and Zn) or due to unequal stress being applied on the surface of the stent. Intragranular corrosion, corrosion within grains, can occur at points of localized deformation or micro cracks developed during processing and handling. Intergranular corrosion, corrosion between grains, can occur at the grain boundaries due to higher available free energy.

In addition to the three different types of corrosion there are three different stages of corrosion for alloys exposed to alkaline chloride solution. First, there is an anodic dissociation growth and absorption of hydrogen bubbles. This is then followed by the development of pitting corrosion (Figure 2). Lastly, there is the growth of an inhibiting film of MgH_2.

In static testing a partial pressure builds up on the surface of the metal. An electron cloud forms on the surface of a metal when the flow is approximately zero. The erosion process is inhibited,

decreasing the rate of corrosion, in effect by changing the composition of the in vivo solution to higher similarity to the base material. Additionally, with a dynamic system, which incorporates fluid flow, the electron cloud is required to reform constantly, which increases the rate of corrosion. Therefore, testing samples dynamically would yield more accurate results on the corrosive behavior of a metal in vivo. Because the exact governing corrosion mechanism varies from alloy to alloy it is important to test the easiest to implement fixes first. Corrosion will occur in the alloy at places containing the highest unstable energy. Because it is difficult to identify where points of local deformation will start within each grain for each individual stent, reducing high energy states between grains becomes an attractive place to start refining. By reducing grain boundaries, through larger grain sizes, areas of high unstable energy are reduced; however, heat treating can allow aluminum within the magnesium matrix to pool into large clusters causing the possibility of galvanic corrosion or areas for localized pitting. This may counteract the benefits given by minimizing grain boundaries. Since the governing corrosion type was unknown, both reducing grain size and growing the grains was tested to try and find a trend.

Grain refinement also offers advantages as a possible solution, as it could easily be tested and implemented within a short time frame. Additionally, grain refinement can provide a final product that is easy to quality control. Less attractive solutions not tested were: alloy changes, coatings such as oxide and polymer, and surface treatments affecting roughness, geometry changes, and single crystal production.

Chapter 4: Procedure

4.1 Procedure Overview

In order to determine the rate of degradation of the magnesium AZ31B rods ASTM G31-72, Immersion Testing for Metals, was used. Using an ASTM standard for magnesium ensures standard practices are maintained. The standard was slightly modified as outlined below but the testing solution and basic premises were held constant. Several types of immersion testing were performed including: static test, a pseudo-dynamic test, and a dynamic test.

Other than an initial degradation test where a 3.5% NaCl solution was used, the rest of the tests were done with 0.9% NaCl*. Adding either 9 grams or 35 grams of reagent NaCl, depending on the concentration needed, and adding as much de-ionized water as necessary to have one liter of solution mixed the solution.

Sample lengths were held constant. Wire cutters were used to cut the samples, and subsequently the ends were ground down using a fine grit sand paper. The lengths of each sample were not recorded, but were approximately targeted to 1.0" ± 0.2" for each static and pseudo-dynamic test. The sample lengths varied in the dynamic test because different geometries were necessary to insert the rods into the tubing. The initial weights of each sample were recorded.

Prior to weighing, each sample was rinsed and wiped down using de-ionized water and ethanol/methanol. Lastly, each sample was dried using a heat gun. This procedure was done on samples before and after immersion into the test tubes. This cleaning method was done to ensure that all contaminants and moisture were removed from the sample that could skew data.

4.2 Static Testing

Static testing was performed using 50 mL tubes with twist on tops, various concentrations of NaCl solution, and a heated water bath. Initially, a static immersion test with a 3.5% NaCl solution at 37°C was performed. The 3.5% NaCl was used in order to have an expedited corrosion rate, and the samples were immersed in a bath at 37°C to mimic in-vivo conditions (Figure 3). Each sample was cut to approximately 1.0" lengths, which corresponded to an average mass of 0.0890 grams with a standard deviation of 0.0033 grams (Table I).

FIGURE 3: 3X7 ARRAY OF 50 ML TUBES FILLED WITH 3.5% NACL SOLUTION INSIDE A BATH WITH WATER KEPT AT 37°C. ONE CUT SAMPLE OF AZ31B WAS PLACED IN EACH TUBE AND REMOVED AT DIFFERENT TIME INTERVALS.

Table I: Initial weights for static immersion testing with 3.5% NaCl at 37°C.

Weight	Day 1	Day 2	Day 3	Day 4	Day 5	Day 6	Day 7
Sample 1	0.0904 g	0.0855 g	0.0937 g	0.0878 g	0.0922 g	0.0858 g	0.0978 g
Sample 2	0.0915 g	0.0851 g	0.0886 g	0.0863 g	0.0893 g	0.0929 g	0.0919 g
Sample 3	0.0877 g	0.0866 g	0.0872 g	0.0895 g	0.0846 g	0.0870 g	0.0878 g

Following the 3.5% test, a 0.9% NaCl solution test was run using the same protocol. Each sample of magnesium was cut to approximate 1.0” and immersed into the 50 mL tubes, and placed into a 37°C bath. The average mass of each sample was 0.0887 grams with a standard deviation of 0.0021 grams (Table II).

Table II. Initial weights for static immersion testing with 0.9% NaCl at 37°C.

Weight	Day 2	Day 3	Day 4	Day 5
Sample 1	0.0916 g	0.0913 g	0.0864 g	0.0893 g
Sample 2	0.0916 g	0.0886 g	0.0873 g	0.0865 g
Sample 3	0.0878 g	0.0865 g	0.0898 g	0.0898 g

For both static tests each sample was removed from its tube on its predetermined day (Table I, Table II), washed and dried, and weighed. Samples were not placed back into their tubes after they were removed. Testing was discontinued based on the condition of the samples. If samples qualitatively appeared to have deep underscoring pitting or measurements seemed skewed by heavy amounts of salt it was determined testing should cease.

4.3 Pseudo-Dynamic Testing Part I

Following the static testing, a pseudo-dynamic test was conducted to determine whether or not liquid flow has an influence on degradation rate. Testing was conducted using: 250 mL beakers, 100 mL of 0.9% NaCl solution, hot plates with stirring capabilities, magnetic stirring rods, parafilm, and a magnesium sample holder (Figure 4). Samples were held immobile against the beaker wall via a polymer coated paperclip and small polymer alligator clamp. Samples were oriented so the end not in the alligator clip was facing oncoming flow.

The pseudo-dynamic testing was conducted at room temperature (~20°C) because the hot plates would heat the NaCl solution to approximately 50°C. To compensate for this temperature change, static testing was performed at room temperature for comparison (Table III). The static testing was performed in the 50 mL tubes with 0.9% NaCl solution, to maintain consistency with the pseudo-

dynamic testing.

FIGURE 4: PSEUDO-DYNAMIC BEAKER AND STIR PLATE. A MAGNETIC STIRRER WAS USED TO SIMULATE FLUID FLOW.

Table III. Initial weights for pseudo-dynamic and static testing of magnesium alloy AZ31-B.

Weight	Pseudo-Dynamic (~20°C)	Static (~20°C)	
Sample 1		0.0936 g	0.0977 g
Sample 2		0.0962 g	0.0977 g
Sample 3		0.0939 g	0.0923 g

4.4 Heat Treatments

In order to refine grain size, 1/16" AZ31B rods were annealed and cooled to three different states following ASTM B661-06. All samples were compared to the as-fabricated AZ31B. In the first treatment AZ31B rods were quenched into cold water at 72° F to reduce grain sizes to as small as possible. In the second treatment AZ31B rods were cooled by leaving samples in the furnace as it cooled to create large grains. In the third treatment AZ31B rods were cooled by air-cooling to create medium sized grains. These rods were then cut into 1.0" pieces and placed into varying in vitro testing environments. Next, samples were cut and mounted for metallography and etched with Kroll's Reagent for 1-5 s. Grain sizes were verified using optical microscopy.

4.5 Pseudo-Dynamic Testing Part II

Following heat treatments, the as fabricated/control, air cooled, furnace cooled and quenched samples were tested in a static and pseudo-dynamic environments (Figure 5).

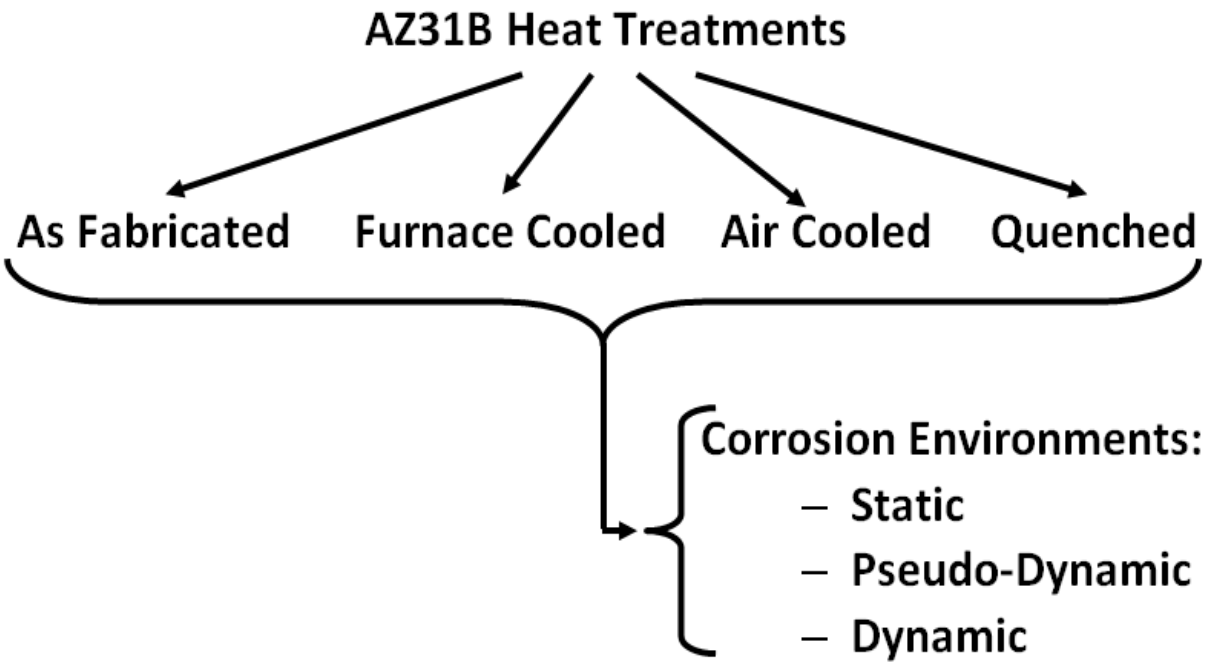

FIGURE 5: CORROSION TREATMENT OVERVIEW. ALL SAMPLES WERE PLACED INTO STATIC AND PSEUDO-DYNAMIC TESTING. ONLY AIR COOLED SAMPLES WERE PLACED INTO FULL DYNAMIC TESTING.

The pseudo-dynamic testing was performed with one sample of AZ31B of each cooling rate in separate beakers on separate stirring plates. These samples were first weighed (Table IV) and then beakers were filled with 250 mL 0.9% NaCl solution. This test was conducted at room temperature (~20°C) because the stirring plate would exceed 37°C, even on its lowest setting. To compensate for this temperature change, two static tests were conducted alongside the pseudo-dynamic test. One of the tests was at 20°C and the other in a water bath at 37°C. Both static tests were done in 50 mL tubes filled with 0.9% NaCl.

Samples were removed from each environment at the same time. Each sample was rinsed with de-ionized water and ethanol/methanol to remove any contaminants that could affect the mass of the samples. The 0.9% NaCl solution was replaced in each test after the samples were pulled. This was done to simulate the arrival of fresh body fluid to the samples.

Table IV: Initial weights for pseudo-dynamic, static (20°C), and static (37°C) of magnesium alloy AZ31B.

Weight	Quenched	Air Cooled	Furnace Cooled	As Fabricated
Pseudo-Dynamic (20°C)	0.0865 g	0.0880 g	0.0863 g	0.0825 g
Static (20°C)	0.0833 g	0.0859 g	0.0833 g	0.0857 g
Static (37°C)	0.0858 g	0.0876 g	0.0871 g	0.0879 g

This testing was repeated a second time for a longer period of time (Table V). All procedures were conducted with the same methods as the first part of testing.

Table V: Initial weights for the Testing 2.

Weight	Quenched	Air Cooled	Furnace Cooled	As Fabricated
Pseudo-Dynamic (20°C)	0.0864 g	0.0835 g	0.0815 g	0.0846 g
Static (20°C)	0.0795 g	0.0785 g	0.0820 g	0.0863 g
Static (37°C)	0.0809 g	0.0783 g	0.0810 g	0.0846 g

4.6 Dynamic Testing

A dynamic model was developed to improve simulating the in vivo conditions that the magnesium stent would be exposed to. The test combined a dynamic flow pump running at approximately 330±10 mL/min, two 1 L beakers filled with 0.9% NaCl, two different sized silicone tubes with inter-diameters of 4 mm and 6 mm and approximately 2 ft. long, a water bath set to 37±1°C, and male/female luer

connectors with barbs for connecting tubing to itself (Figure 6).

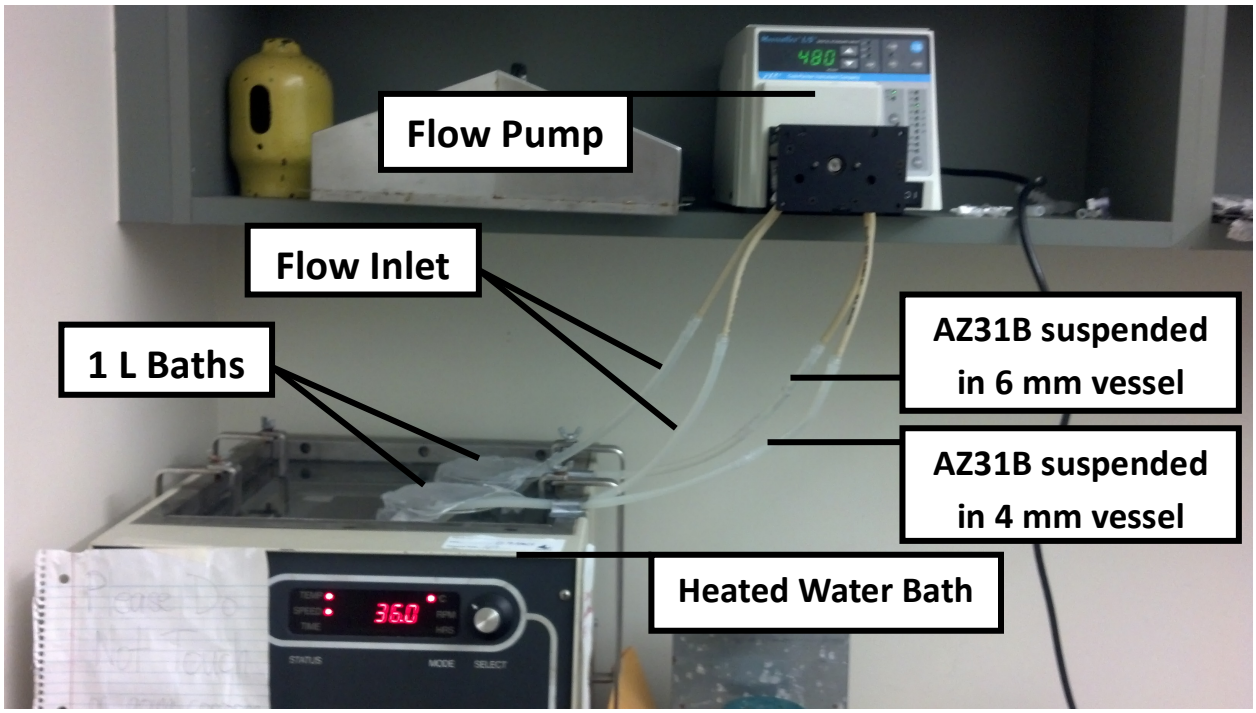

FIGURE 6: EXPERIMENTAL SET-UP FOR DYNAMIC TESTING OF MAGNESIUM ALLOY SAMPLES.

The silicone tubing was cut into two sections: the flow inlet side and the outlet side. The samples were suspended in the outlet side using a 3-5" piece of silicone tubing and luer connectors with barb fittings. Samples of AZ31B were bent by hand and suspended in the 4 and 6 mm silicone vessels. The 6 mm vessel allowed for a ring shaped bend and two straight sections on either end to stay wedged within the vessel. The 4 mm vessel didn't allow for a ring to be bent within it. Therefore, an alternative shape was considered, and the middle of the sample was be bent up to wedge the sample within the tube, while keeping the ends of the sample straight (Figure 6).

The silicone tubing, luer connectors and the magnesium sample were weighed before dynamic testing because the samples were difficult to remove when they needed to be weighed. Each item was weighed separately to obtain an accurate initial weight. The system with the sample added were weighted together and the time dependent mass of the sample determined by subtraction (Table VI).

All dynamic testing was conducted using air cooled heat treated samples. This decision was based on rough estimations determining that the air cooled heat treatment had the slowest degradation in a pseudo-dynamic environment. Initially only one sample was used for each vessel diameter (Table VI).

Samples were dried and cleaned by rinsing the entire sample set-up with de-ionized water followed by an ethanol/methanol rinse and drying with a heat gun and compressed air. Samples were considered dry when no more moisture was visibly seen, and moisture was no longer leaving the set-up using compressed air.

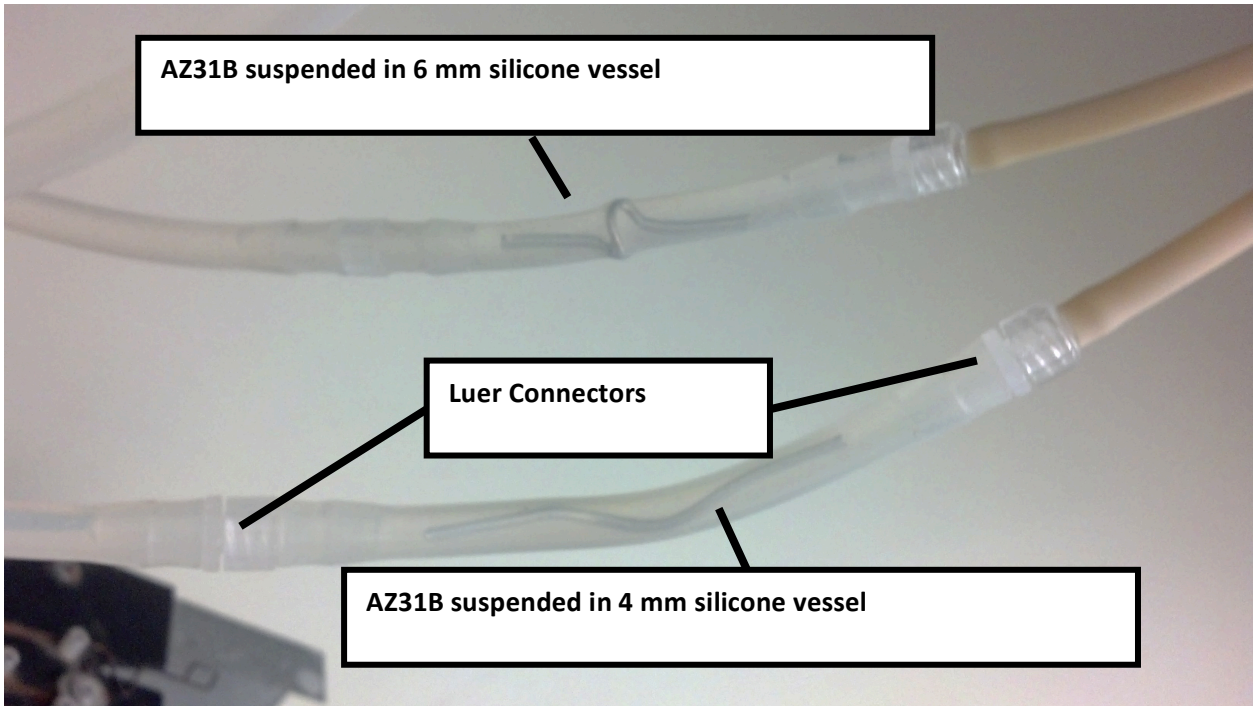

FIGURE 7: CLOSE UP OF THE DIFFERENT CONFIGURATIONS OF MAGNESIUM SAMPLES FITTED INTO 4 AND 6 MM SILICONE VESSELS.

Table VI: Initial weights of dynamic testing samples.

Vessel ID	Silicone Tube (g)	Barb Connectors x2 (g)	Mg Sample (g)	Total (g)
6 mm	4.5202	1.35	0.2691	6.1273
4 mm	4.8924	1.16	0.2489	6.3300

Secondary dynamic testing was performed by connecting three sample chambers together in series (Figure 8). It was decided that the samples wouldn't have a major effect on each other within the same vessels due to the solution to sample ratio being used. In order to simulate a more in vivo environment water baths of 1 L were used. Therefore, the concentration gradient of magnesium ions within solution would be less than if 50 mL or 100 mL of solution were used (static and pseudo-dynamic testing solution amounts). This allowed for the increased sample size within each test.

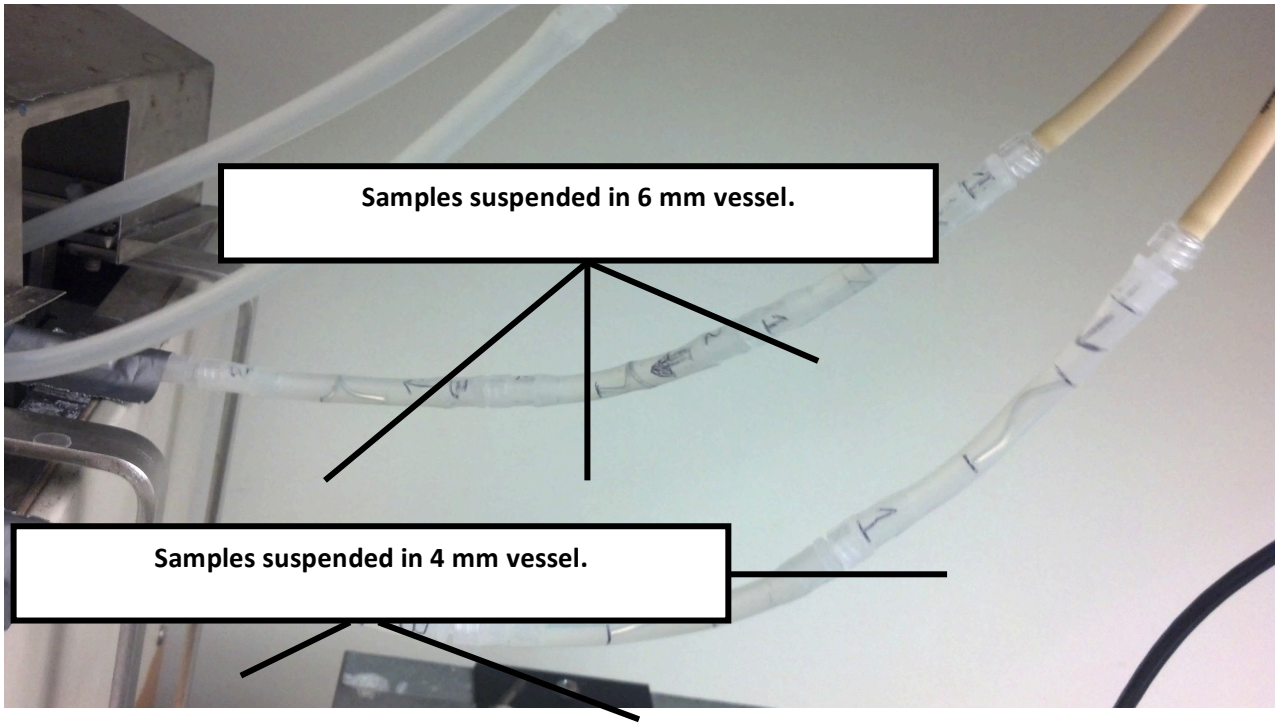

FIGURE 8: EXPERIMENTAL SET-UP OF 6 & 4 MM VESSEL DYNAMIC TEST WITH THREE SAMPLES CONNECTED IN SERIES.

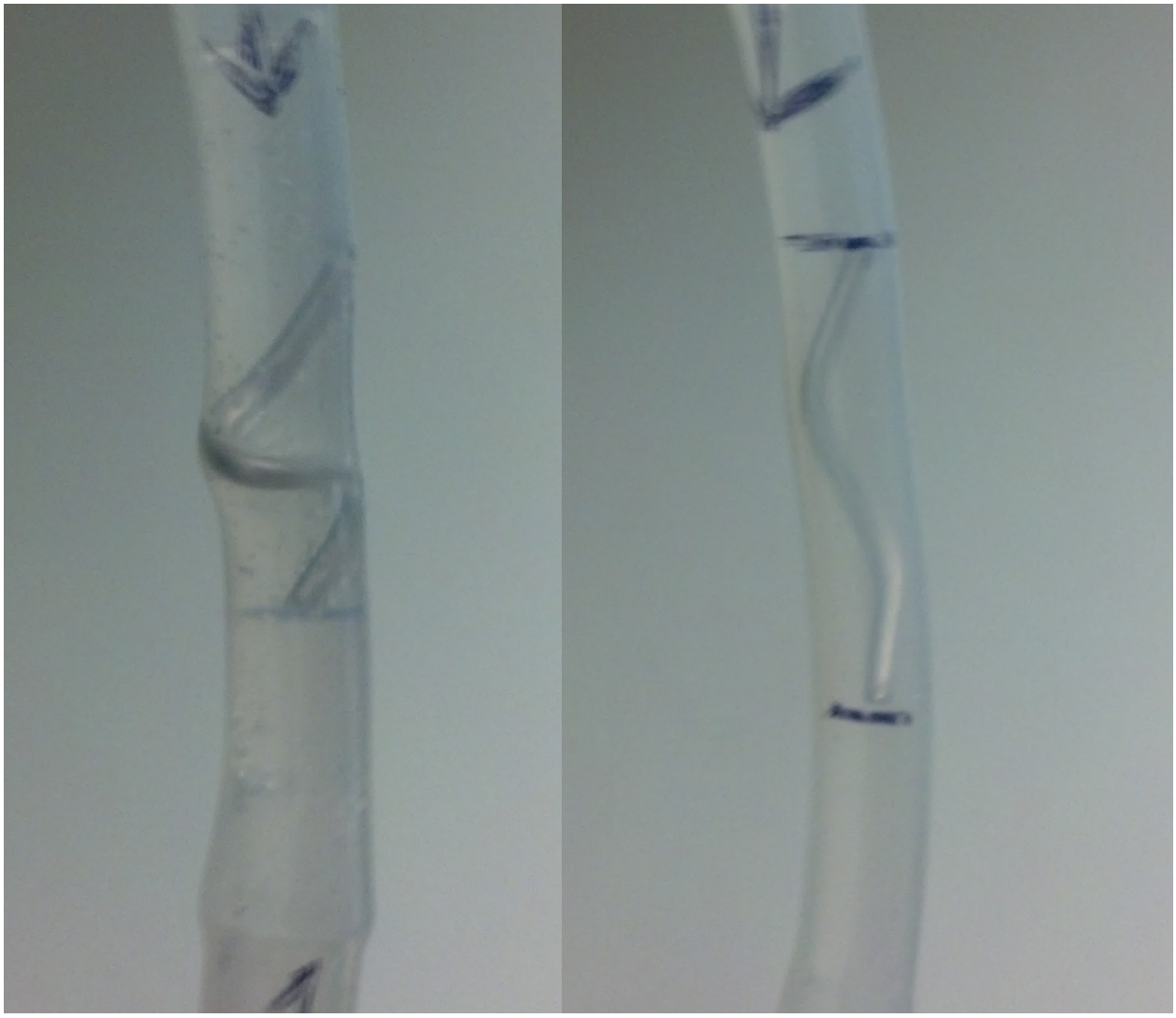

FIGURE 9: CLOSE UP VIEW OF 6 MM (LEFT) AND 4 MM (RIGHT) VESSEL DEPICTING THE DIFFERENT ORIENTATION AND GEOMETRIES OF THE MAGNESIUM SAMPLES.

Magnesium samples and the test set-up were initially weighed in order to obtain mass loss information from the testing (Tables VII-VIII). Samples were removed on various days. Each sample was dried and weighed.

Table VII: Initial weight of 6 mm vessel samples.

6 mm Vessel	Sample 1 (g)	Sample 2 (g)	Sample 3 (g)
Magnesium Sample	0.1188	0.0965	0.0955
Total Initial Weight	5.1667	5.2244	5.4507

Table VIII: Initial weight of 4 mm vessel samples.

4 mm Vessel	Sample 1 (g)	Sample 2 (g)	Sample 3 (g)
Magnesium Sample	0.1136	0.0973	0.1056
Total Initial Weight	5.8479	5.6672	5.4612

Chapter 5: Results and Discussion

5.1 Heat Treatments

Preliminary heat treating resulted in the following microstructures (Figure 4) and grain size properties (Table IX). Heat treatments reduced grain size by an average of 3 um, from 10.78 um as received samples. However, cooling rate has no significant effect on grain size manipulation, as show below in Figure 11. Control AZ31B samples exhibit heterogeneous grain distribution and size. Heat treated samples exhibit homogenized the grain size and distribution.

Table IX: Grain sizes and etchant times for each sample.

	As Fabricated	Quenched	Air Cooled	Furnace Cooled
Average Grain Size	10.76um	7.818um	7.56um	7.79um
Date of Test	9-May	9-May	9-May	9-May
Etchant	Krolls Reagent	Krolls Reagent	Krolls Reagent	Krolls Reagent
Method	3-5s	3-5s	3-5s	3-5s
Magnification	1000x	1000x	1000x	1000x
Number of fields	1	1	1	1
Field area	4.65 mm^2	4.65 mm^2	4.65 mm^2	4.65 mm^2

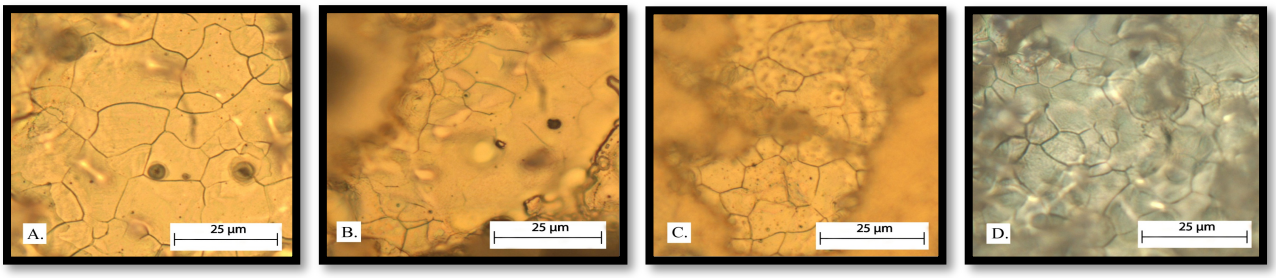

FIGURE 10: HEAT TREATED MICROSTRUCTURES. FROM LEFT TO RIGHT: AS FABRICATED/CONTROL, AIR COOLED, FURNACE COOLED, AND QUENCHED. GRAINS WITHIN THE "AS FABRICATED" ARE SIGNIFICANTLY LARGER THAN THE OTHER TREATMENTS.

Due to the different sizes of samples it was necessary to standardize all the sample weights to attain useful data. It was determined that a percent mass loss calculation was the necessary method to attain this useful data (Calculation 1).

[(initial mass – final mass)/(initial mass)] * 100 = % mass loss **Calculation 1**
[(0.09 g – 0.08 g)/(0.09 g)] * 100 = **11.1%**

5.2 Static Testing

Initial static testing was done on as fabricated magnesium samples at 37°C in 3.5% NaCl solution. This testing showed an increased rate of corrosion (Figure 11). The average of each days mass loss was taken, and converted to a mass remaining in percent. Samples degraded between 40%-60% after 7 days. If an exponential curve is fit to the average data it would show that the magnesium would no longer remain after approximately 25-30 days.

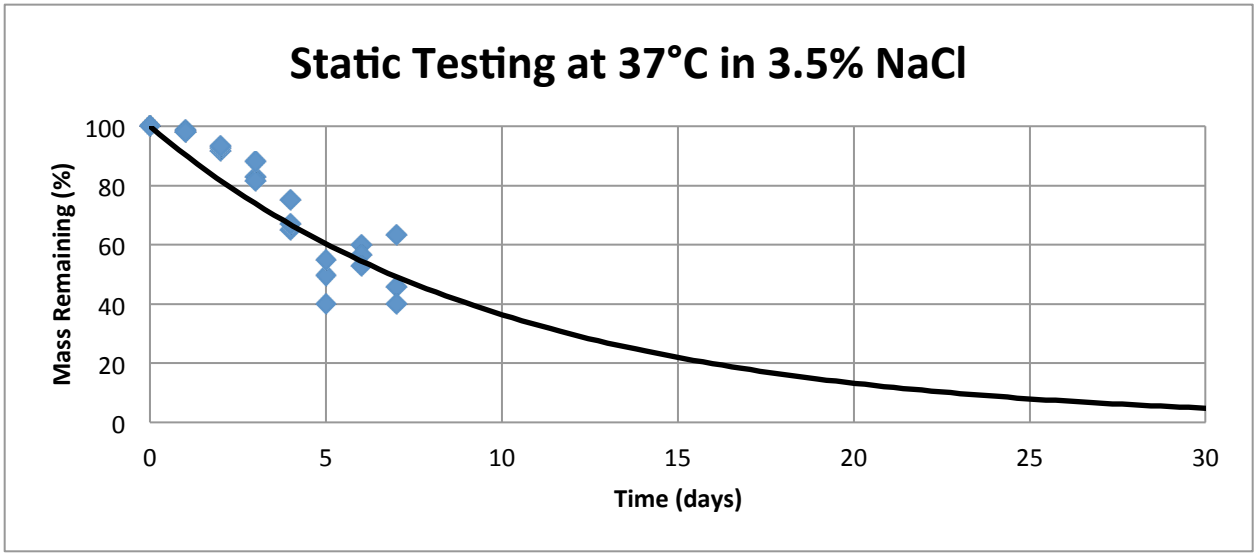

FIGURE 11: INITIAL STATIC TESTING AT 37°C IN 50 ML TEST TUBES FILLED WITH 3.5% NACL SOLUTION. SAMPLES WERE TAKEN OUT ON A DAILY BASIS FOR SEVEN DAYS, AND AN EXPONENTIAL CURVE WAS FIT TO THE AVERAGE OF EACH DAYS REMAINING MASS.

To mimic a more in-vivo environment, static testing was repeated in the same way, but with 0.9% NaCl solution instead of 3.5% NaCl solution (Figure 12). Samples degraded between 86% and 96% after 5 days in 3.5% NaCl compared to between 40% and 55% after 5 days in the 0.9% NaCl. An average of each days mass remaining was calculated, and an exponential curve was fit to the data. It shows that at approximately 150-200 days the magnesium sample would be close to non-existent.

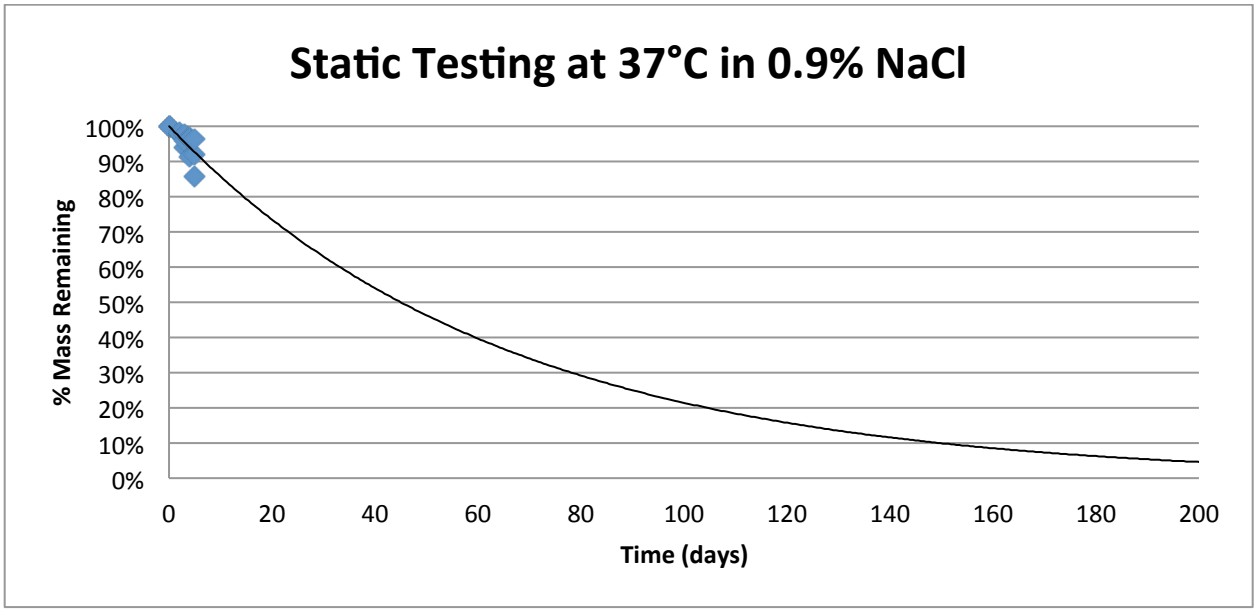

FIGURE 12: SECONDARY STATIC TESTING AT 37°C IN 50 ML TEST TUBES FILLED WITH 0.9% NACL SOLUTION.

5.3 Pseudo-Dynamic Testing Part I

A pseudo-dynamic test was conducted on the as fabricated magnesium samples next (Figure 13). Figure

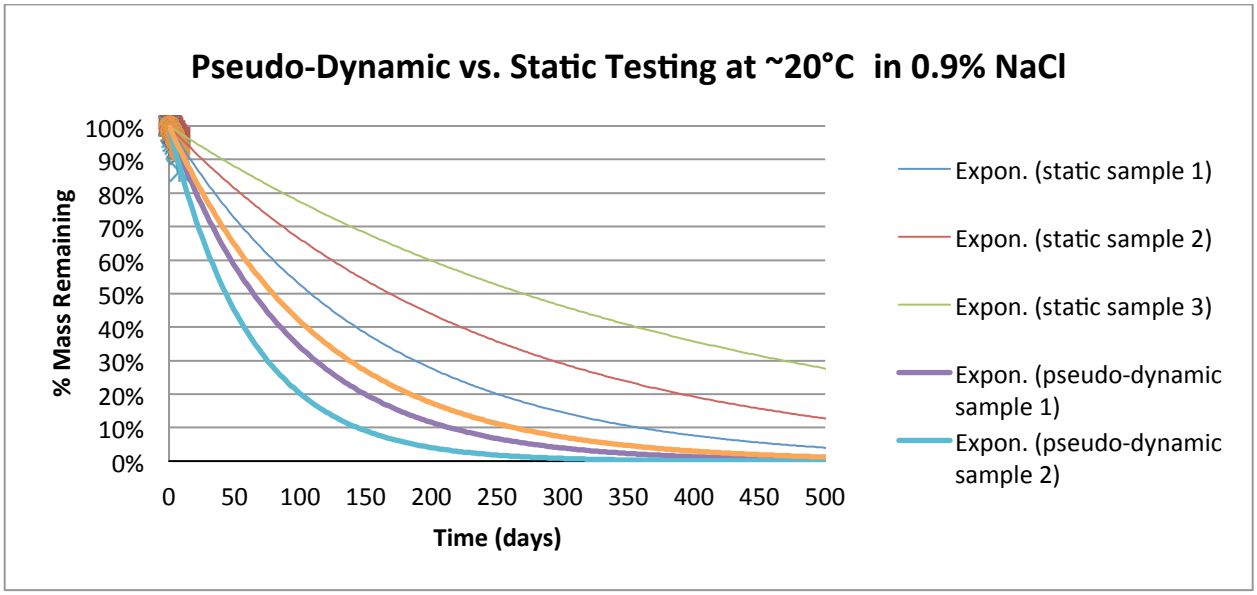

FIGURE 13: PSEUDO-DYNAMIC VERSUS STATIC TEST AT ~20°C IN 0.9% NACL SOLUTION. THE PSEUDO-DYNAMIC TEST WAS CONDUCTED WITH 100 ML OF NACL IN A 250 ML BEAKER AND THE STATIC TEST WAS CONDUCTED IN A 50 ML TEST TUBE.

This test further mimicked in-vivo conditions by simulating flow over the magnesium samples, and was compared to a static test run at room temperature. There was no applicable way to do a long-

term pseudo-dynamic test at 37°C; therefore, the test was run at room temperature. Pseudo-dynamic samples degraded between 86% and 92% after 8 days compared to 95% and 98% for the static samples after 8 days. By extrapolating the data using an exponential curve it was found that the pseudo-dynamic samples would degrade after approximately 150-250 days and the static samples would remain from 350-600 days.

5.4 Pseudo-Dynamic Testing Part II

Additional pseudo-dynamic comparison tests followed, but were run with samples exposed different heat treatments. The heat treatment for each sample was the same, but the cooling rates were different for each sample. The different cooling rates were quenched, air cooled, and furnace cooled. These heat treatments were tested against the as fabricated, control, magnesium samples. In an initial pseudo-dynamic test run at room temperature in 0.9% NaCl the quenched sample had 87% of its mass remaining after 7 days, the air cooled had 90% remaining, the furnace cooled sample had 83% remaining and the as fabricated sample had 86% remaining. This test was compared to a static room temperature test and static 37°C test. The static room temperature test showed the quenched sample had 93% mass remaining, the air cooled had 95% mass remaining, the furnace cooled had 94% mass remaining, and the as fabricated sample had 89% mass remaining. The 37°C static test showed the quenched sample had 88% mass remaining, the air cooled had 86% remaining, the furnace cooled had 85% remaining and the as fabricated sample had 82% mass remaining. Each test was run for 7 days. Samples were removed for measurements at day 3 of testing.

To gain a better understanding of the pseudo-dynamic testing, another test similar to the previous test was conducted. The difference in this test was the duration of the test. The test was run for 16 days and samples were pulled at 4 days and 10 days. The tests conducted were a static test at ~20°C, a static test at 37°C, and a pseudo-dynamic test at 37°C.

The static testing in room temperature showed that the quenched sample had 85% mass remaining after 16 days, the air cooled sample had 87% remaining, the furnace cooled had 74% remaining, and the as fabricated sample had 80% remaining (Figure 14).

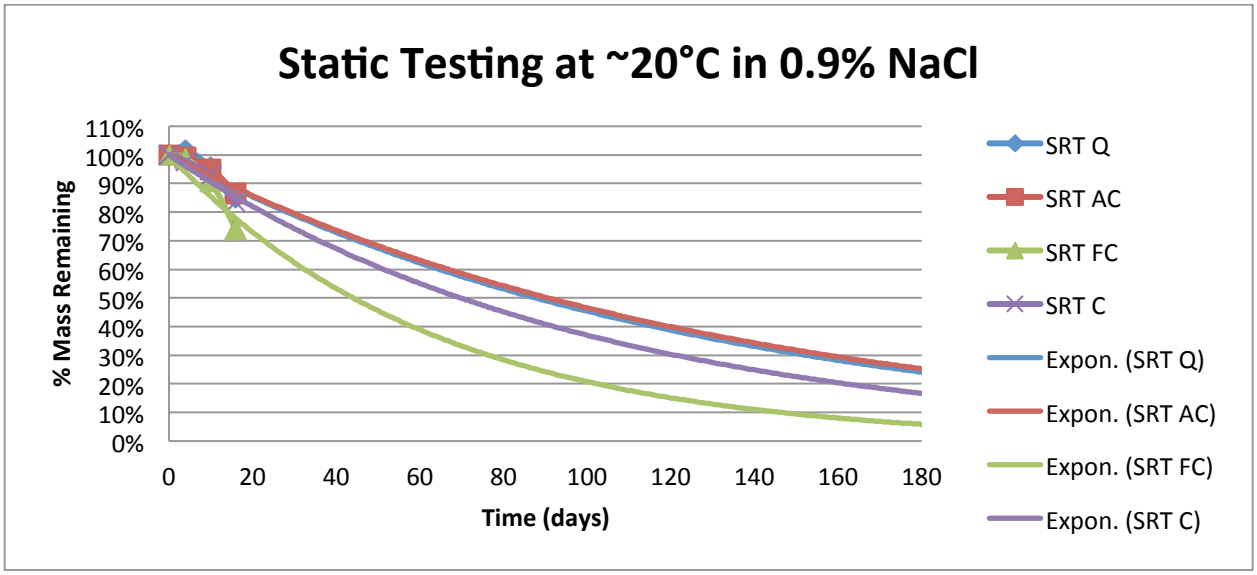

FIGURE 14: STATIC TESTING AT ~20°C RESULTS FOR 16 DAYS, EXTRAPOLATED USING AN EXPONENTIAL FUNCTION.

The static testing at 37°C showed that the quenched sample had 57% mass remaining after 16 days, the air cooled sample had 75% remaining, the furnace cooled had 68% remaining, and the as fabricated sample had 80% remaining (Figure 15).

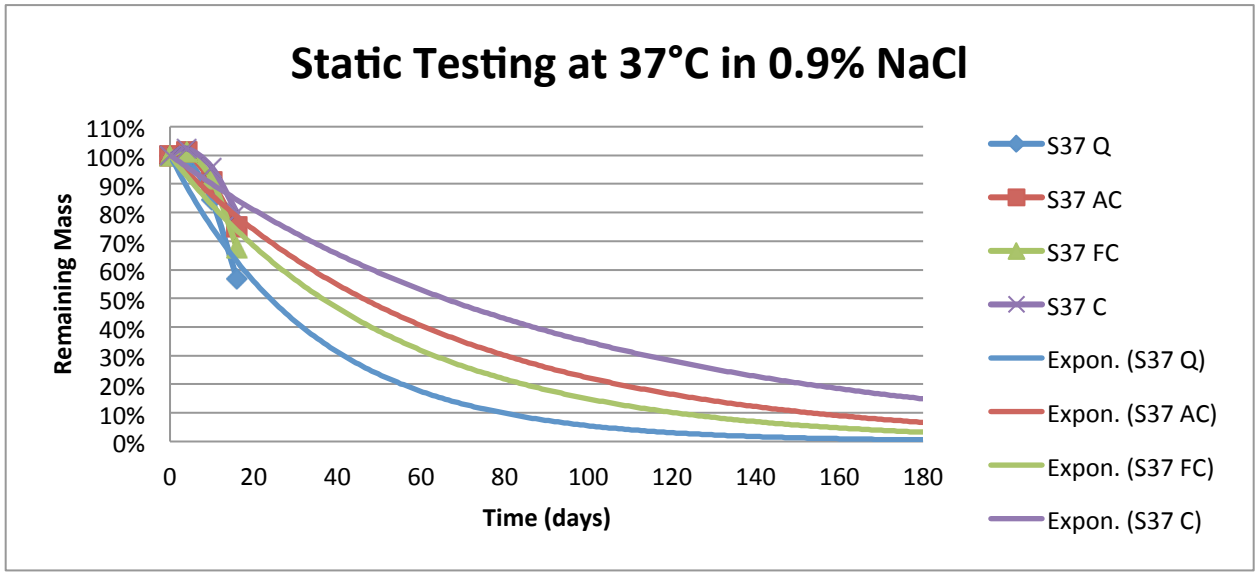

FIGURE 15: STATIC TESTING AT 37°C RESULTS FOR 16 DAYS, EXTRAPOLATED USING AN EXPONENTIAL FUNCTION.

The pseudo-dynamic testing at ~20°C showed that the quenched sample had 53% mass remaining after 16 days, the air cooled sample had 69% mass remaining, the furnace cooled sample had 73% mass remaining, and the as fabricated sample had 80% mass remaining (Figure 16).

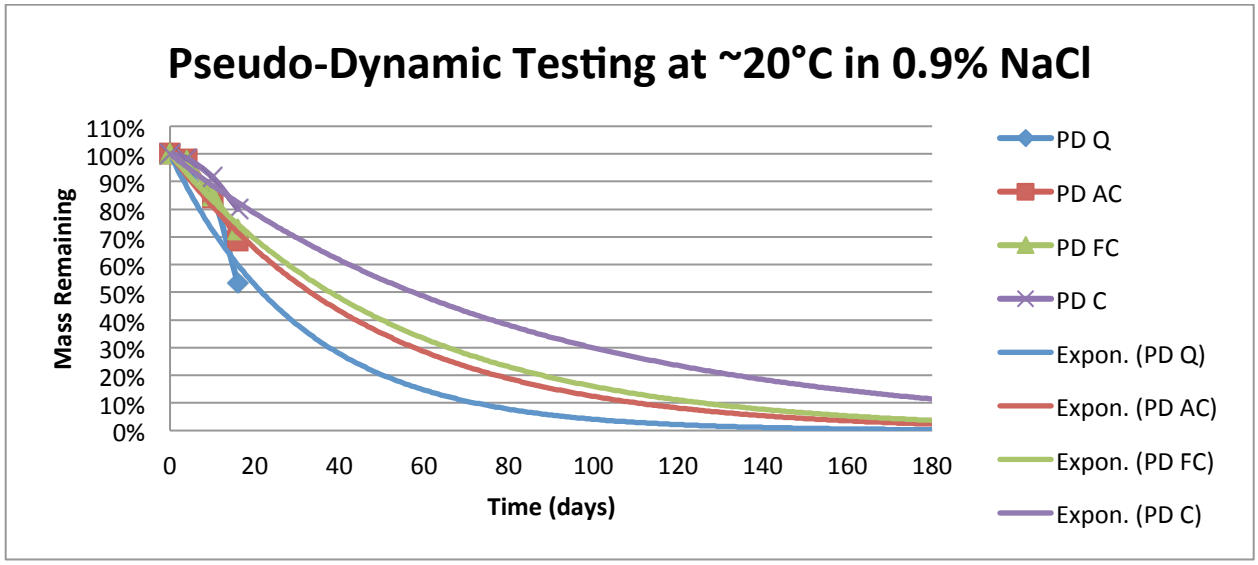

FIGURE 16: PSEUDO-DYNAMIC TESTING AT ~20°C RESULTS FOR 16 DAYS, EXTRAPOLATED USING AN EXPONENTIAL FUNCTION.

5.5 Dynamic Testing

A dynamic test was conducted to more accurately simulate the in vivo environment. The different vessel sizes tested were 6 mm and 4 mm inter-diameter silicone vessels. Both tests were run side by side. Air cooled samples were chosen to be tested because of their improved performance in the previous testing. Three samples were placed in each vessel diameter. The samples were first fitted into a vessel chamber, which could be attached to other samples in series, and to the rest of the set up, as well (Figure 8). Samples were pulled at 4, 7, 12, and finally 19 days. The 0.9% NaCl solution was not changed between removals.

The 6 mm vessel data showed that the air cooled magnesium sample would have between 63% to 67% mass remaining after 19 days (Figure 17).

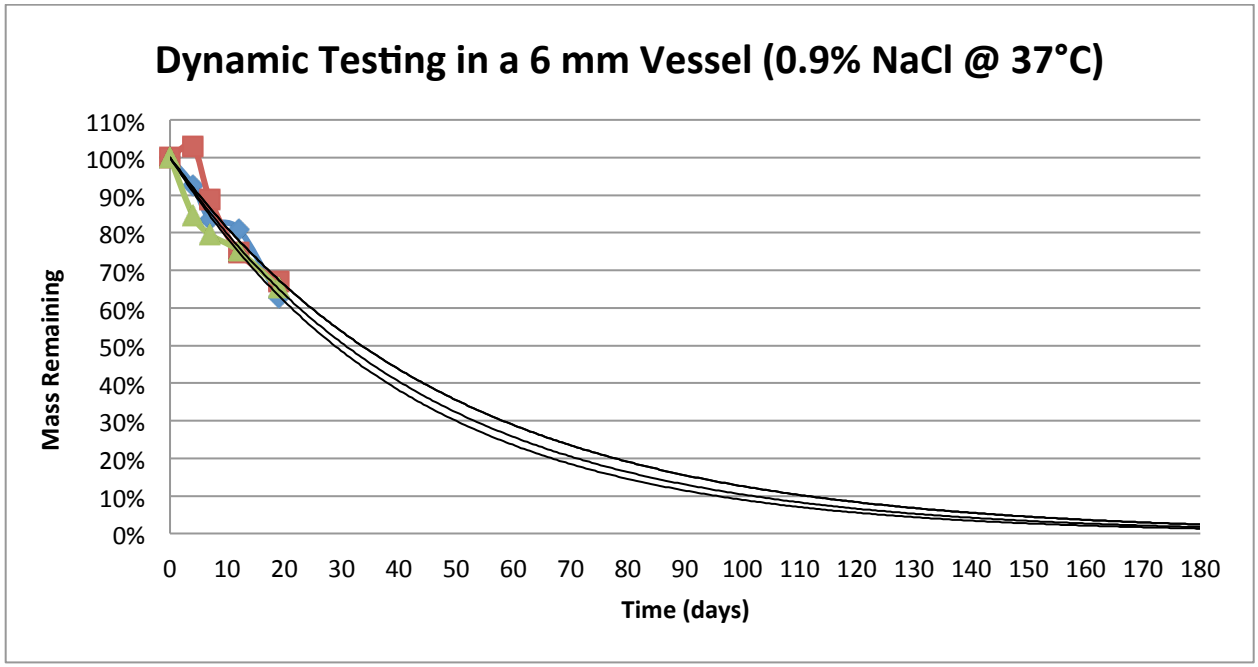

FIGURE 17: THREE SAMPLES OF HEAT TREATED AND AIR COOLED MAGNESIUM TESTED IN A DYNAMIC FLOW MODEL AT 37°C IN 0.9% NACL SOLUTION.

The 4 mm vessel data showed that the air cooled magnesium sample would have between 51% and 73% mass remaining after 19 days (Figure 18).

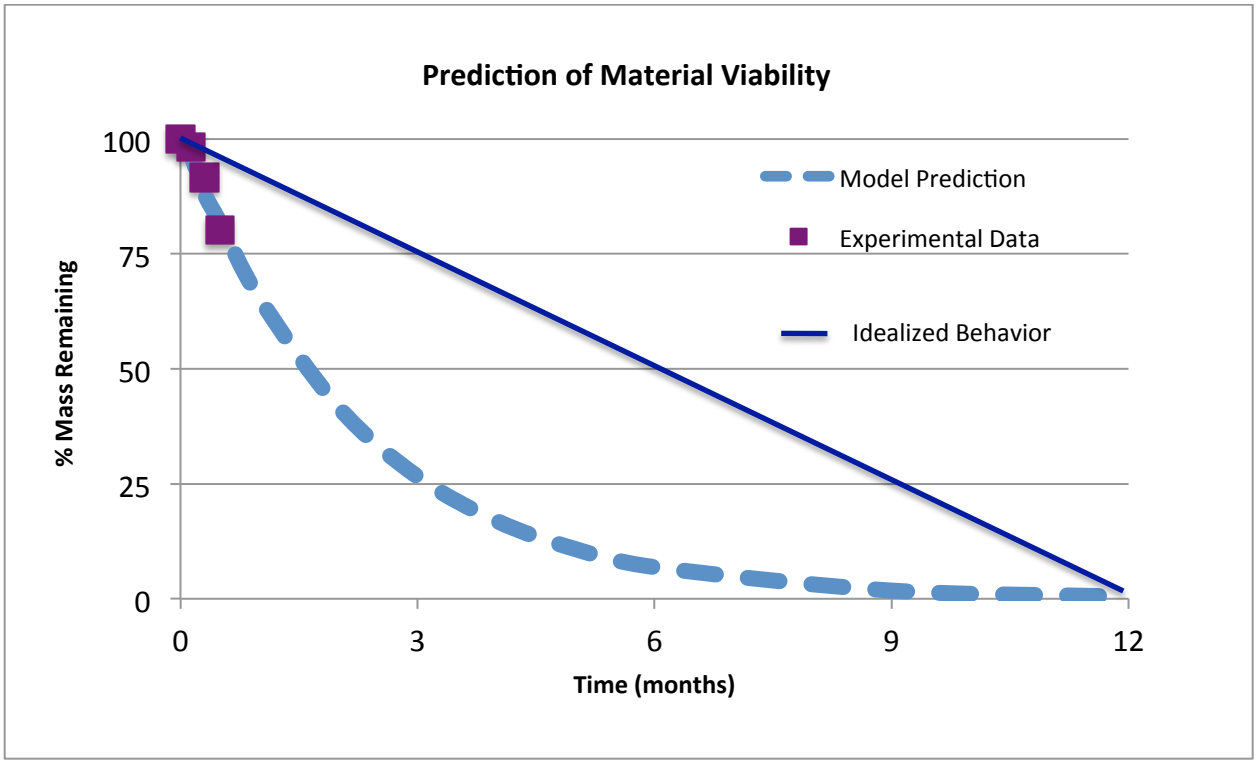

FIGURE 18: THREE SAMPLES OF HEAT TREATED AND AIR COOLED MAGNESIUM TESTED IN A DYNAMIC FLOW MODEL AT 37°C IN 0.9% NACL SOLUTION.

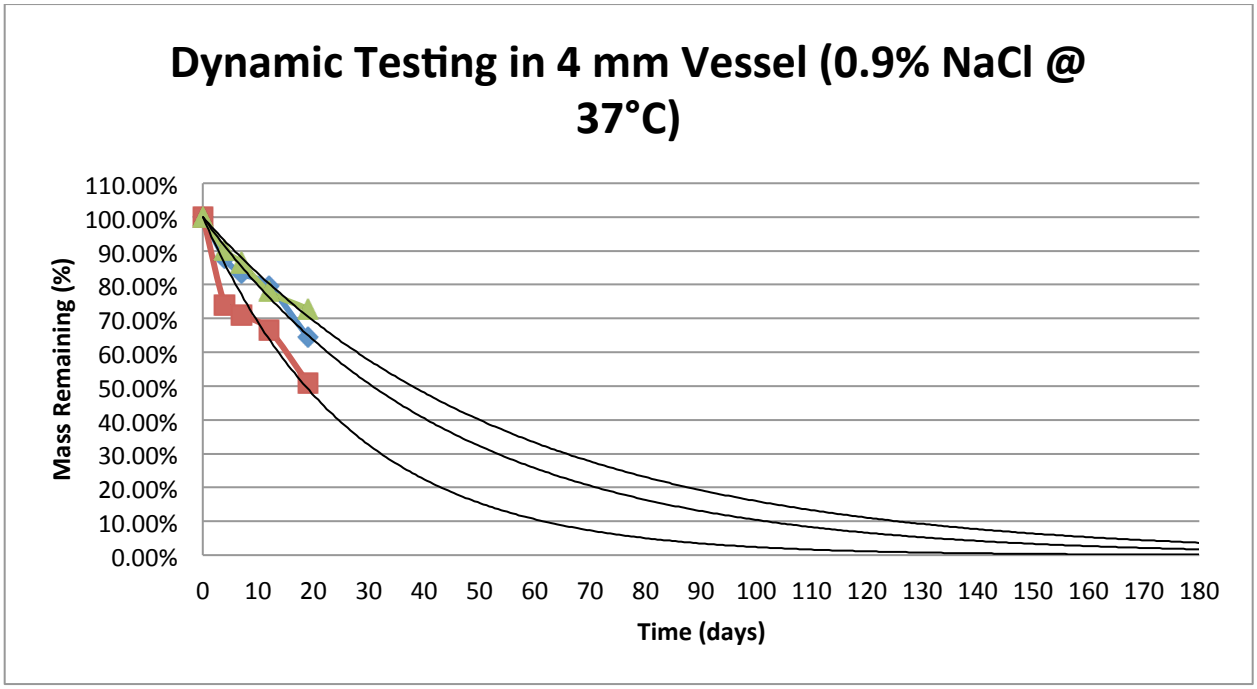

FIGURE 19: COMPARISON OF THE MODEL PREDICTION, IDEALIZED BEHAVIOR, AND EXPERIMENTAL DATA.

5.6: Initial Discussion of Experimental Data

Given our heat treatments, it was apparent grain size would not be decreased below the 7.5 um threshold due to temperature at which the samples were elevated to given ASTM XXX. Control samples are speculated to have large, less homogenized grain structure due to the as fabricated processing, which includes hot rolling at elevated temperatures for extended periods of time. It's hypothesized that the as received samples where held at significantly longer times than samples used for degradation control testing resulting in larger, distorted grains observed under optical microscopy.

Through testing, as received samples exhibited longer, more uniform degradation rates. This is speculated to be caused from the larger grain size, that in turn results in a structure with less dense grain boundaries. Grain boundaries are a preferred nucleation point for corrosion due to their high-energy states relative to other parts of the microstructure. Therefore, as fabricated samples have fewer initiation points for corrosion, and should naturally degrade in a more controlled matter which was observed during all testing.

Due to small physical sample size in heat treatments, it's possible that prior to the different cooling methods, upon opening furnace door its possible the temperature within the magnesium fell below the recrystallization temperature, therefore abstaining further grain growth from occurring. However, this was not verified, and was not considered during analyzing microstructures.

The primary form of corrosion experienced within our samples on the macro scale was random localized pitting. Because corrosion is a highly unpredictable form of degradation, even more so with magnesium, its possible the AZ31B samples experiences multiple forms of degradation and not solely degradation from pitting. However, given optical examination of corroded samples, pitting appeared to be the primary contributor.

Given quantitative and qualitative experimental data, magnesium alloy AZ31B proved to be a poor choice for stenting material due the unpredictable and non-uniform nature of the materials ability to corrode. Given the electromotive force series, magnesium is the most anodic (active) metallic material. And because AZ31B is magnesium alloyed primarily with aluminum and zinc, micro galvanic cells are created with a high difference in electrochemical potential between metals. The micro galvanic

cells formed are randomized, making corrosion difficult to pin point. And due to the randomized nature, non-uniform corrosion is a problem as observed in every tested sample.

Chapter 6: Discussion

Degradation is the result of both erosion and corrosion. Therefore, it is necessary to characterize both parameters to predict changes in stent thickness over time. A predictive corrosion model is presented in the next chapter. The aims of the modeling include 1) analysis of the corrosion experiments, 2) development of a predictive corrosion model, and 3) prediction of shear stresses using finite element analysis (FEA) for future erosion models.

.

6.1 Experimental Data

The experimental pseudo-dynamic control equation (Chapter 4) was plotted with an exponential curve fit (Figure 20), determined to be the experimental corrosion rate, and used as the data set for subsequent discussion.

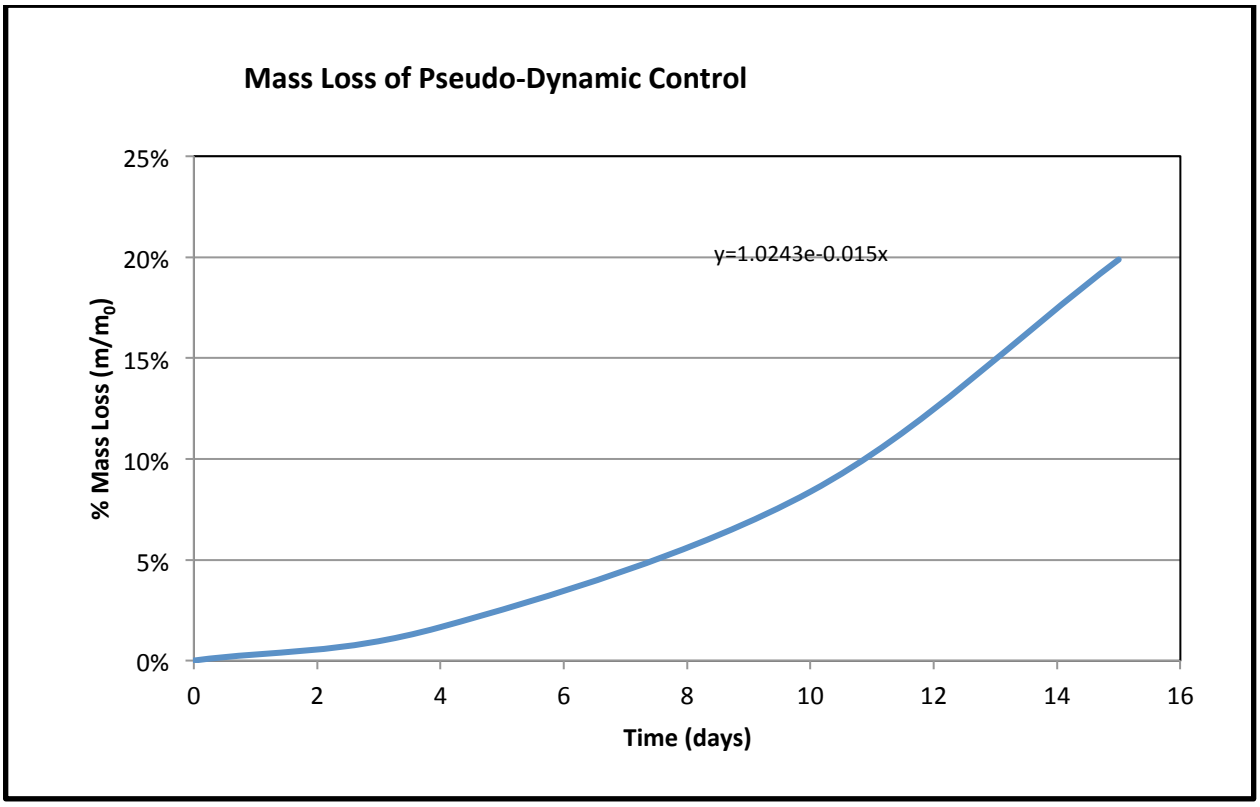

FIGURE 20: ILLUSTRATION OF THE EXPONENTIAL RATE OF DEGRADATION OF THE PSEUDO-DYNAMIC CONTROL GROUP.

This is expected due to corrosion effect where the galvanic reactions become more active over time as surface area increases on the material. The rate equation determined by the mass loss of the

pseudo-dynamic control data was used in Section 6.2 to predict the changes of stent geometry owning to corrosion by extrapolation of this data set.

6.2 Prediction of Stent Geometry Change Owing to Corrosion

Corrosion can be modeled using a mass balance, which predicts degradation as a function of time by characterizing for geometric changes. A complex mathematical model was developed to elucidate the effects of corrosion and erosion individually on degradation. The mathematic model was not successful in predicting degradation rates, but is considered useful for further development of this project by future students. Additional information for the mathematical model can be found in Appendix D. However, a simplified mass balance was created to predict the change in mass of the stent with time, and used to determine the dominating factor of degradation. The thickness prediction as a function of time is shown in equation 1.

$$\frac{dm}{dt} = -R_{exp} \qquad \text{(Equ. 1)}$$

where R_{exp} is the experimental corrosion rate. Integrating both sides, inserting the experimental corrosion rate, and solving for constants provides the following equation:

$$t = \frac{1}{b}\ln\left[\left(\frac{m}{m_o} - 1 - \frac{A}{bm_o}e^{bt}\right) * \left(-\frac{bm_o}{A}\right)\right] \qquad \text{(Equ. 2)}$$

where m_o is the initial material mass, m is the mass remaining at time t, A, b and C are constants, and t is the time required for mass m. Additional details can be found in Appendix C.

The mass balance equation predicts the percent of material remaining over time. This is illustrated in Figure 21. Table X presents a numerical prediction of stent presence remaining in the vessel over time.

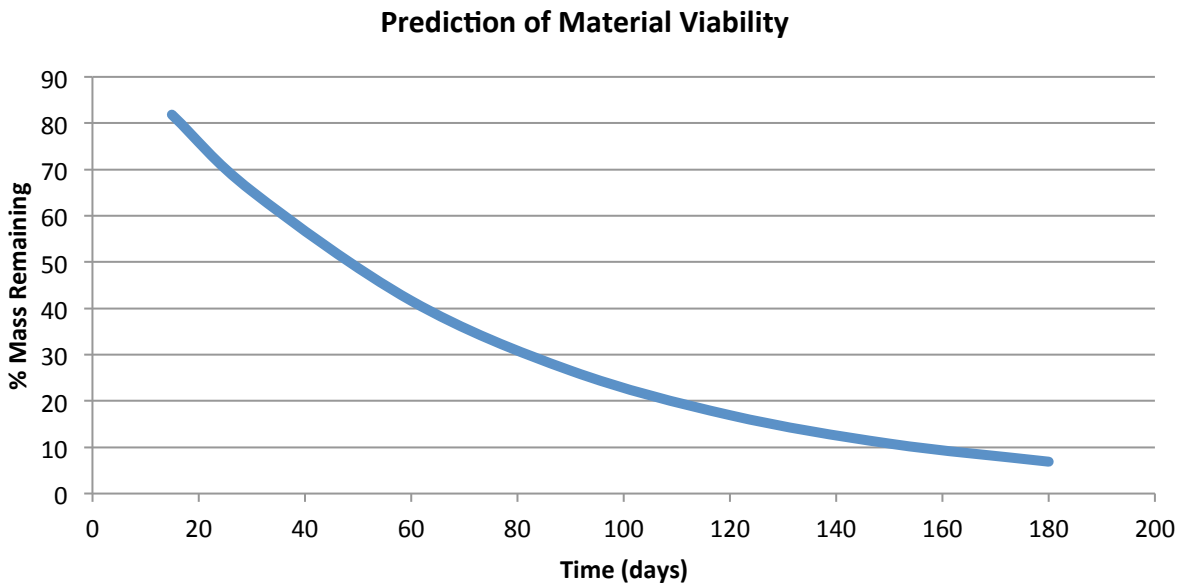

FIGURE 21: MASS LOSS OF MATERIAL FROM BULK OVER TIME.

Table X: Prediction of mass remaining at critical time points.

% Mass Remaining	Evaluation Day
81.792	15
65.312	30
26.554	90
6.884	180

The experimental data yielded an average of 81.193% material remaining at 15 days, which closely relates to the predicted value of 81.792%, yielding and average of 1.96% difference between the experimental data and the mathematical model. The mass balance therefore indicates that corrosion and not erosion effects dominate degradation.

The time requirement set by Medtronic for product lifetime was approximately 6 months after implantation. The mass balance estimates 6.884% of the original mass will remain at 6 months. Theoretically the metallic alloy will still be present in the vessel at 6 months; however, this does not ensure that adequate mechanical properties are maintained, nor does it address geometric changes and the effects changes in geometry have on flow patterns. It is important to also note that none of these

predictions take into account biological factors such as protein adsorption and cell adhesion, which can also alter degradation rates of a material.

6.3 Prediction of Stent Geometry Change Owing to Erosion

Previous sections addressed the effects of corrosion on degradation, but erosion is also a factor that alters degradation rates of materials. The underlying theory to describe the influences of shear stress on rates of erosion is beyond the scope of this report. However, it is known that degradation due to erosion depends on local shear stresses. We performed FEA to determine blood flow rates and shear stresses acting on struts and the exposed endothelial lining. Further detailed simulation set up and analysis can be found in Appendix B.

6.3.1 Geometry

The model was created in a 2D axisymmetric geometry that models a 2D geometry as a 3D model by revolving the 2D around a symmetry boundary. The geometry was created using COMSOL, and all dimensions were determined based on literature values [8]. The geometry and the dimensions are illustrated in Figure 22.

6.3.2 Set-up and Simulation

Flow in the arteries is pulsatile. Therefore, the flow was modeled as laminar, incompressible, Navier-Stokes flow. This module assumes that the density of the fluid, blood, is constant and considered to be incompressible. The simulation was run using a coarse mesh and assuming the simplified waveform: $(1+\Phi\sin(\omega t))$. This model is only dependent on the pressure the fluid expresses, the location of the stent within the artery tree, the frequency of the fluid flow, and the time the model is run. From these assumptions and parameters, the velocity profile of the vessel with the implanted stent and the magnitude of the shear stress at points along the stent struts were determined and analyzed.

6.3.3 Results and Discussion

To discuss the relationship between flow and shear stress influences, five points are defined in Figure 23. Points A and E correspond to the junction between the stent strut and endothelial lining. Points B and D correspond to the top and bottom of the strut, respectively. Point C corresponds to the strut apex.

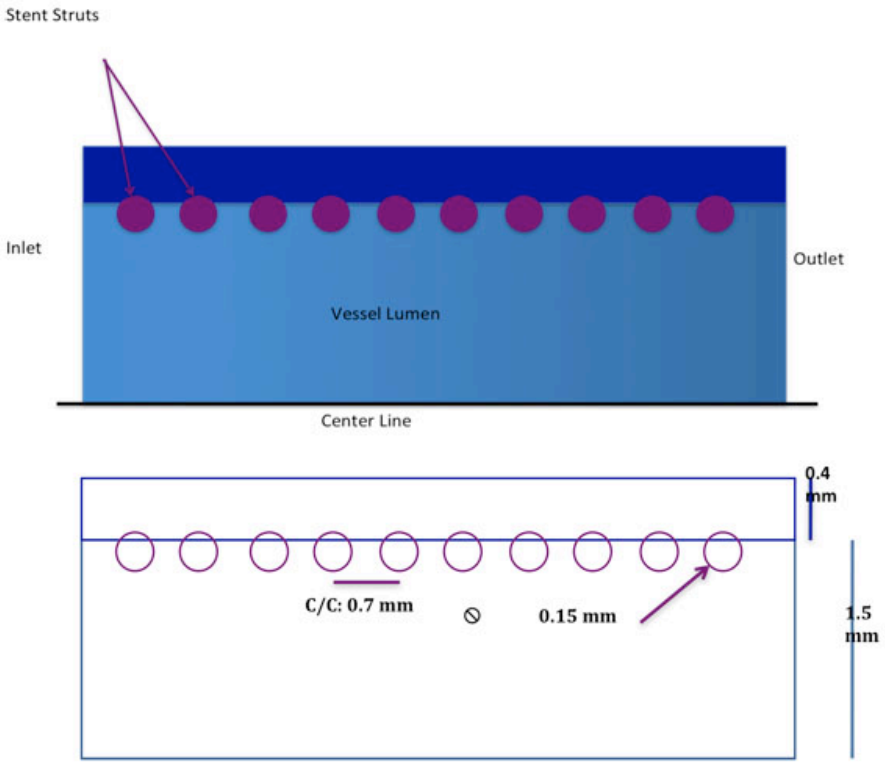

FIGURE 22: SCHEMATIC OF THE COMPONENTS OF THE COMPLETE VESSEL MODEL WITH DIMENSION.

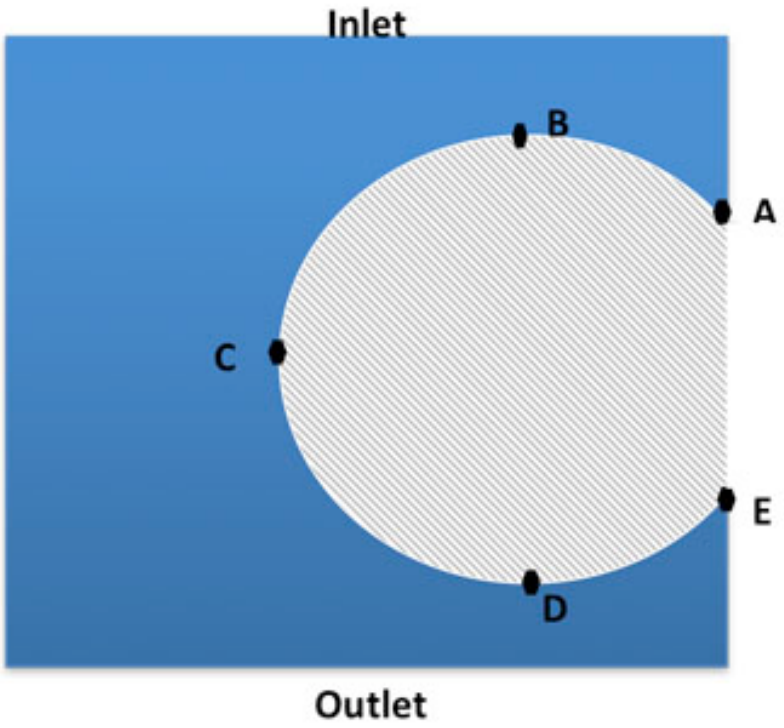

FIGURE 23: SCHEMATIC OF ANALYZED STENT POSITIONS IN COMSOL

The velocity profile of the vessel and struts characterizes changes in flow due to the stent implant. Changes in velocity can influence degradation rates, shear stresses, and the favorability of cell and molecular adhesion to the endothelial lining and the stent struts [11]. Figure 24 shows a color plot of the velocity profile of the vessel and stent.

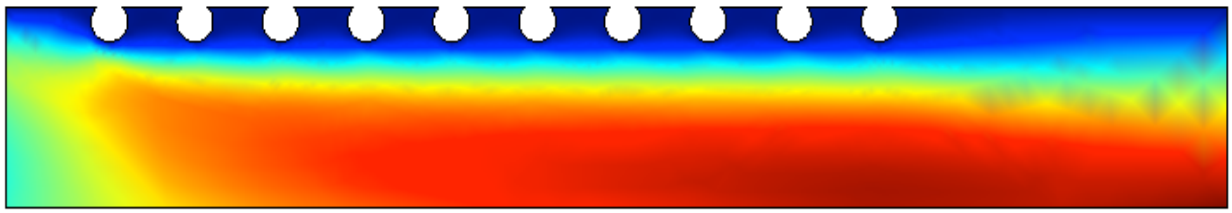

FIGURE 24: COLOR PLOT OF VELOCITY PROFILE OF THE STENT AND STRUT WHERE RED INDICATES THE GREATEST VELOCITY AND BLUE THE LOWEST MAGNITUDE OF VELOCITY.

The color plot indicates the greatest flow occurs at the lumen center, and the lowest magnitude of velocity is at the vessel wall. It is important to notice that the stent interrupts normal flow patterns at the inlet and increases the depth of the region of reduced flow along the vessel wall. Alterations in the

flow pattern can alter corrosion rates. It is possible to utilize FEA studies to determine optimal geometry of the struts to maintain a desired velocity in the vessel.

Atherosclerosis is most prominent in regions of disturbed flow and decreased shear stress. Shear stress is directly related to cell shape and function. Endothelial shear stress (ESS) is a possible predictor of atherosclerosis and restenosis due to stenting. A minimum shear stress is required to satisfy the endothelial cells at the wall of the lumen. Without adequate shear stress, restenosis is possible at an increased rate and scar tissue is more likely to form. Scar tissue decreases the elasticity of the vessel, which adds to the effects of heart disease [11]. A color plot of the shear stress profile is shown in Figure 25.

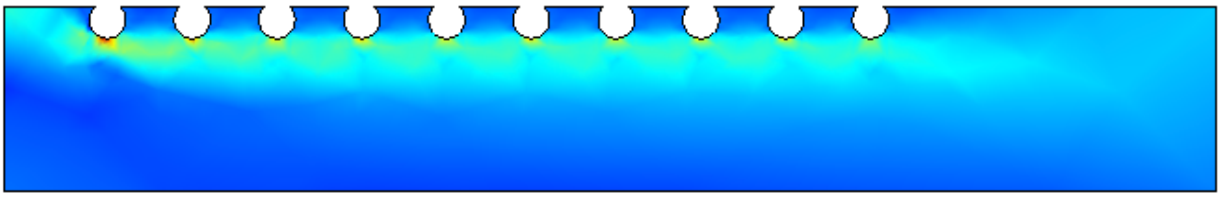

FIGURE 25: COLOR PLOT OF SHEAR STRESS WHERE RED INDICATES THE GREATEST MAGNITUDE OF SHEAR STRESS AND BLUE TO LOWEST MAGNITUDE.

The shear stress experienced at the strut is variable with respect to position. The greatest magnitude of shear stress is experienced at position C. Positions A and E experience shear stresses of approximately zero, which indicates the endothelial cells do not experience adequate shear stress for optimal viability. Shear stress according to position remains approximately consistent after the first four or five struts for all positions. This is illustrated in Figure 26.

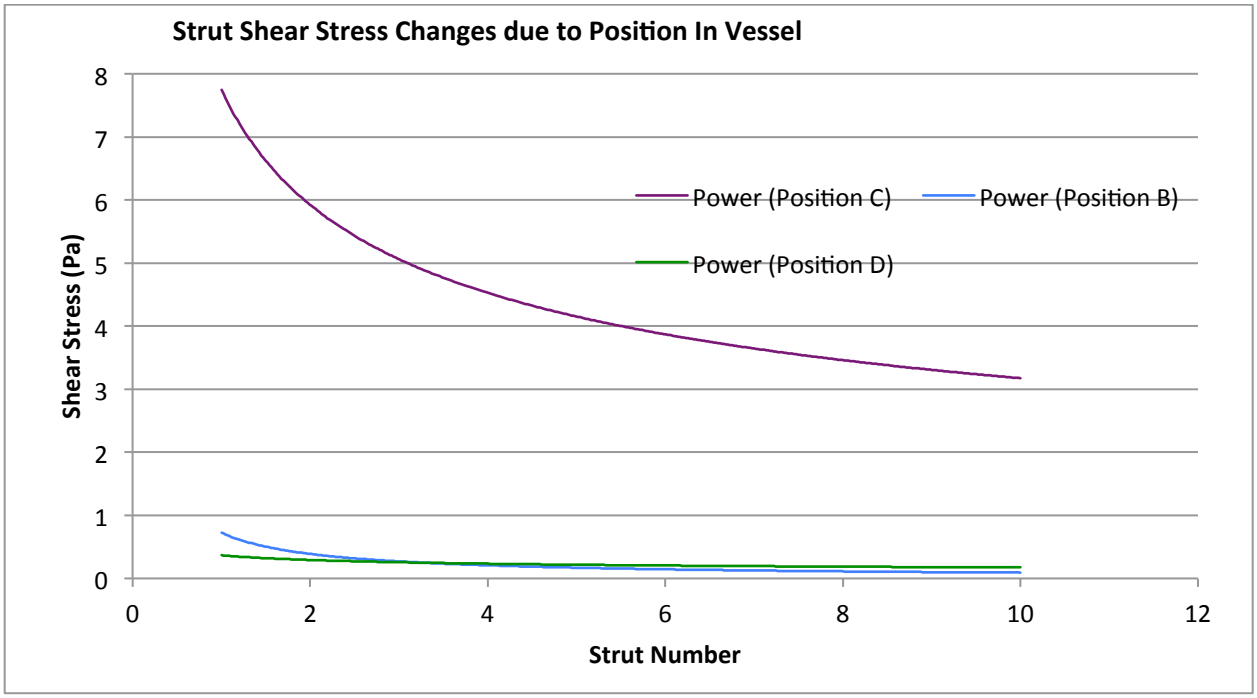

FIGURE 26: SHEAR STRESS AS A FUNCTION OF STRUT NUMBER ALONG THE VESSEL LENGTH FOR POSITIONS B, C, AND D.

Because the stent experiences increased shear stress at the proximal region than the distal region of the stent, restenosis will increase in stents with increased length. Difference WSS experienced at each evaluated position of the stents would result in non-uniform corrosion of the struts. Positions B and D would corrode at a slower rate than position C, which experiences the greatest magnitude of shear stress. Additionally, the change in WSS at each position for the first 4 or 5 struts would results in variant corrosion rates for these first struts, where the corrosion rate would be the same for each strut after the first 4 or 5 initial struts. Therefore, the stent should be designed to accommodate the greatest magnitude of shear stress accommodated, which accelerates corrosion. This way the stent would be designed to meet the minimum time requirement for the functional presence of the stent.

Changes in shear stress directly relate to vascular homeostasis and remodeling effects. The mean WSS in the arterial system is 15-20 dynes/cm^2 [11]. However, deviations from a baseline are more significant than a standard WSS magnitude. EC dysfunction is attributed to decreases in WSS, which results in decreased EC regulation and increased SMC proliferation. These all contribute to the probability of a restenosis event. Therefore, it is necessary to understand the effects of flow on EC. This can help to researchers understand the development of vascular pathologies such as atherosclerosis and in-stent restenosis that results from stent implants. Design optimization is possible by developing stent geometries that limit flow disturbance around the stent and promote healthy levels of WSS.

Critical WSS is defined in literature as less than 1.26 Pa [11]. The regions of cells surrounding the stent do not experience WSS values that meet this minimum. Therefore, these regions are at increased risk of restenosis. Stenting, in all cases, decreases the WSS below the optimal level for maintaining stress on the endothelial cells, and results in stagnation in regions surrounding the struts.

Chapter 7: Conclusions

- Magnesium alloy AZ31B is not a viable material to be used as a stent without modification.
- Magnesium alloy AZ31B exhibits non-uniform, highly variable forms of corrosion.
- Variable cooling rates from 350°C proved no significant effects on grain size; therefore, these treatments did not help to control corrosion characteristics.
- Control samples exhibited slower, more controlled degradation characteristics due to their larger size grains.
- Dynamic fluid flow proved to be more randomized, and more accelerated relative to static modeling.
- The primary form of degradation observed was corrosion rather than erosion.
- Samples directly in contact (tension) with vessel wall was observed to exhibit more controlled degradation.
- Samples corroded differently in a static environment, pseudo-dynamic environment, and fully dynamic environment.

Chapter 8: Future Applications

- It may be possible to optimized stent strut and spacing to decrease altered flow environment to decrease the event of restenosis.
- For a controlled, more uniform degradation, investigate a polymer-metallic composite material.
- Develop method to accurately quantify material loss.
- Investigate effects of corrosion with magnesium sample held in tension.
- Continue to develop the mathematical model that separately evaluates the factors contributing to degradation.
- Develop a more accurate waveform for FEA simulations.
- Investigate effects of deployment on the magnesium material during angioplasty and balloon expansion.
- Explore effects of various surface modifications and the effects of corrosion.
- Develop a theory to describe the influences of shear stress on rates of erosion.
- Continue dynamic immersion testing in alternate solutions to better mimic the in vivo environment.

Appendix A: References:

1. Cochelin, B. Dumoulin, C., 2000. Mechanical behavior modeling of balloon-expandable stents. Journal of Biomechanics 33, 1461-1470.
2. Dee, K.C., D.A. Puleo, and R. Bizios. *An Introduction to Tissue-Biomaterial Interactions.* Hoboken: WileyLiss, 2002.
3. Dehlaghi, V., et al. 2008. Analysis of wall shear stress in stented coronary artery using 3D computational fluid dynamic modeling. Journal of Materials Processing Technology 1197, 174-181.
4. Hagemeister Jens. "Compliance of cobalt chromium stent alloy- the COVIS trail." In *Curr Controls Trials Cardiovac Med.* 2005; 6(1): 17.
5. H. M. Wache, D. J. Tartakowska, A. Hentrich and M. H. Wagner. "Development of a polymer stent with shape memory effect as a drug delivery system" *Journal of Materials Science: Materials in Medicine Volume 14, Number 2",* 109-112, DOI: 10.1023/A: 1022007510352
6. J. Vander Sloten, P. Verdonck, M. Nyssen, J. Hauesen (Eds.): ECIFMBE 2008, IFMBE Proceedings 22, pp. 2175-2178,2008
7. Kereiakes DJ, Cox DA, Hermiller JB, Midei MG, Bachinsky WB, Nukta ED, Leon MB, Fink S, Marin L, Lansky AJ., Guidant Multi-Link Vision Stent Registry Investigators Usefulness of a cobalt chromium coronary stent alloy. Am J Cardiol. 2003;92:463–6. doi: 10.1016/S0002-9149(03)00669-6.
8. Lim, I.A.. "Biocompatibility of Stent Material." *MURJ: The MIT Undergraduate Research Journal* Vol. 11; Fall 2004.
9. Mejia, Juan et al. "Evaluation of the effect of stent strut profile on shear stress distribution using statistical moments." BioMedical Engineering OnLine. April 30, 2009. (stent dimensions for COMSOL)
10. "Modeling Guide." COMSOL AB. November 2008. pp. 134-151.
11. Ormistron, John A. Serruys, Patrick W.S. "Bioabsorbable Coronary Stents." Circulation: Journal of the American Heart Association. June 2009, pp. 255-260. (existing devices and technologies section)
12. Stone, Peter H. et al. "Effect of Endothelial Shear Stress on the Progression of Coronary Artery Disease, Vascular Remodeling, and In-Stent Restenosis in Humans: In Vivo 6-Month Follow-Up

Study." Circulation: Journal of the American Heart Association. July 14, 2003. pp. 437-444 (necessary endothelial stress info)

13. Temenoff, J.S, and A.G. Mikos. “Biomaterials.” In *The Intersection of Biology and Materials Science,* 1st ed. New Jersey: Pearson Prentice Hall, pp. XX –XX, 2008.
14. Waksman, Ron. "Update on Bioabsorbable Stents: From Bench to Clinical." Journal of Interventional Cardiology. 2006, pp. 414-421. (initial clinical trials)
15. Williams, D.F. *The Williams Dictionary of Biomaterials.* Liverpool: Liverpool University Press, 1999.
16. Williams, D.F. and R.I. Williams. “Degradation Effects of the Biological Environment on Metals and Ceramics.” In *Biomaterials Science: An introduction to Materials in Medicine,* B.D. Ratner, A.S. Hoffman, F.J. Schoen, and J.E. Lemons, Eds., 2nd ed. San Diego: Elsevier Academic Press, pp. 430-439, 2004

Appendix B:

B.1 Additional COMSOL Set-Up Instructions

COMSOL is an FEA software package that uses numerical methods and coupled physics to solve complex geometries and systems. COMSOL is capable of creating interactions between modules. For this project, the microscale electro-mechanical systems (MEMS) module was used to interact with the computational fluid dynamics (CFD) module to model the microfluidics of the vessel-stent system. The MEMS module is capable of assessing the fluid-structure interactions between the stent, blood vessel wall, and the blood. Material properties can be assigned to the stent struts in this module. The CFD module assesses complex fluid flow simulations through the lumen of the vessel and the MEMS module interacts to assess fluid-structure interactions between the blood, stent and vessel lining. COMSOL allows for drawing capabilities of vessels and stent structures, and also allows imports of geometries from SolidWorks and other CAD-based programs. Ideally, the desired geometry would be created in a CAD program, imported into a 3D model of the vessel in COMSOL and characterized as a comprehensive simulation.

B.1.1 Geometry

The geometry was created using COMSOL, and all dimensions determined based on literature values [8]. The model of the stent and vessel were drawn in three sections. The lumen radius was determined to be 1.5 mm. Each stent strut was circular with a radius of 0.15 mm and inlaid 0.01 mm into the endothelial lining. The stent struts protrude into the flow field. This offset value of 0.01 mm acts to mimic the diameter of the stent after deployment, where the stent is embedded in the endothelial lining. The endothelial layer was determined to be 0.4 mm. Each stent strut as spaced 0.7 mm from the center of each neighboring strut. The geometry is shown in Figure 27, and the dimensions in Figure 28.

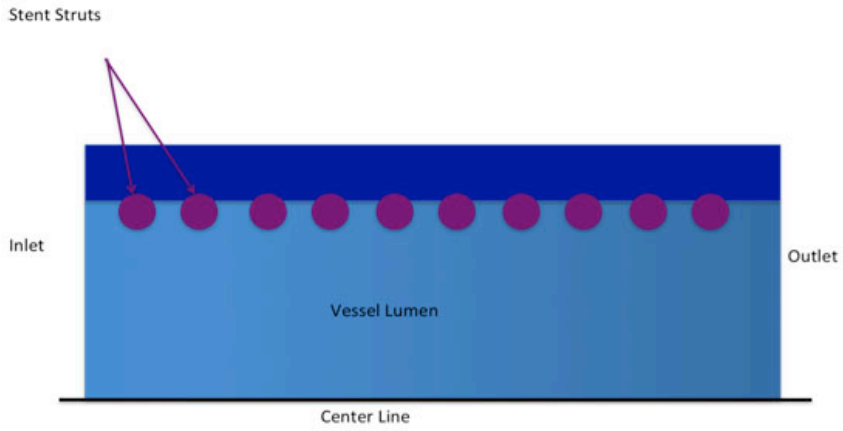

FIGURE 27: SCHEMATIC OF THE SIMPLIFIED GEOMETRY EVALUATED IN COMSOL.

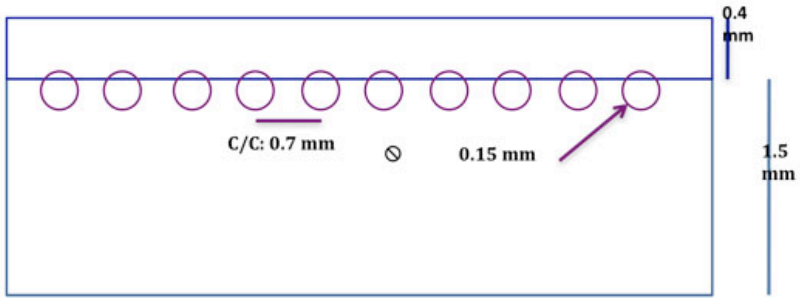

FIGURE 28: DIMENSION OF THE GEOMETRY EVALUATED IN COMSOL.

An array tool was used to create multiple, identical stent struts along the length of the vessel and the stent struts were differenced out of the model by creating composite objects. This was a simplification and assumes that the struts and endothelial lining have infinite stiffness. Therefore, this assumes that the properties of both the stent struts and endothelial lining are irrelevant to this model. With adequate computer capabilities, an ideal situation would allow material properties to be assigned to the stent struts, which would allow for more accurate evaluations of the effects on the material from flow. Additionally, the endothelial layers alter the radial stress on the struts and have individual, unique properties, which would affect the shear stress experienced at the interface between the stent, lumen and lining. This was simplified and drawn as a single layer of endothelial with identical properties.

B.1.2 Boundary Conditions

The following assumptions were made:

- No slip at the walls. The fluid at the wall is stationary.

- The outlet pressure was set to zero, indicating no viscous stress. This assumes the length of the vessel is long enough to establish normal flow past the stent structure.
- Phi = 0.35. Phi is the dampening coefficient of the pulsatile waveform of blood through the vessel. This is a fractional value determined by the placement of the stent within the artery tree.
- The viscosity for the artery is u=3.0 cP.
- The density of blood is 1,060 $\frac{kg}{m^3}$.
- Axial symmetry was applied to all boundaries with the coordinate r=0, or the centerline.

The following equations were used to determine initial conditions:

- Average vessel velocity:

$$< v > = \frac{(P_1 - P_2)h^2}{3\mu l}$$

where <v> is defined as the average velocity, P_1 the initial pressure, P_2 the final pressure, μ is the viscosity of blood, h is the dermis height.

- Pressure drop across a vessel:

$$Q = \frac{\pi R^4 \Delta P}{8\mu l}$$

where Q is the flow rate, R is the radius of the vessel, L is the length of the vessel

- Transient waveform:

$$Waveform = (1 + \Phi * sin(\omega * t))$$

where Φ is defined as the dampening coefficient, ω is equal to 2πf, and f is the frequency of pulsation

- Shear stress:

$$T_{rz} = -\frac{udv}{dy}\Big|_{y=h}$$

- The inlet pressure condition is determined by:

$$P_i = \Delta P \ * \ (1 + \Phi * sin(\omega * t))$$

B .1.3 Solver Settings

A compromise between efficiency and accuracy is required when choosing an appropriate time step to evaluate transient solutions. Increasing computational work is required for larger Δt.

COMSOL uses a generalized version of the Navier-Stokes equations to solve for parameters and assumes, at minimum, conservation of momentum. These equations are in terms of transport properties and velocity gradients. The first equation is the momentum transport balance based on Newton's Second Law and the second is an equation for continuity of an incompressible fluid [9].

B.1.4 Simulation

The intravascular flow characteristics were determined by solving transport equations governing conservation of mass and momentum. The simulation was run assuming the simplified waveform: (1+Φ*sin(ω*t)). In the future it would be appropriate to evaluate the FEA model using a more realistic waveform specific to the region of implant within the artery tree. A unstructured, extremely course mesh was used. The simulation was run for 1 minute with time step intervals of 0.05 minute. This correlates to 120 intervals per minute of simulation.

B.2 Mesh Refinement Study

The accuracy of the model can be improved via mesh refinement. Increasing the refinement of the mesh increases the number of degrees of freedom, which provides a more accurate solution. However, the higher the element order and the larger the degrees of freedom the greater the memory required to produce a solution. Local mesh refinements at the wall provided improved accuracy at the point where the shear stress and velocity profile are expected to be more complex. An unstructured, inhomogeneous, coarse mesh was used for this simulation.

As an experiment, the simplified model discussed in Section X was used to elucidate the effects of mesh refinement on simulation accuracy. All parameters were held constant in successive simulations except for the mesh quality surrounding the stent region. A very course mesh setting

was used for all simulations, but a finer mesh near the region of importance was implemented. Figure 29 illustrates the importance of the mesh in evaluating a model.

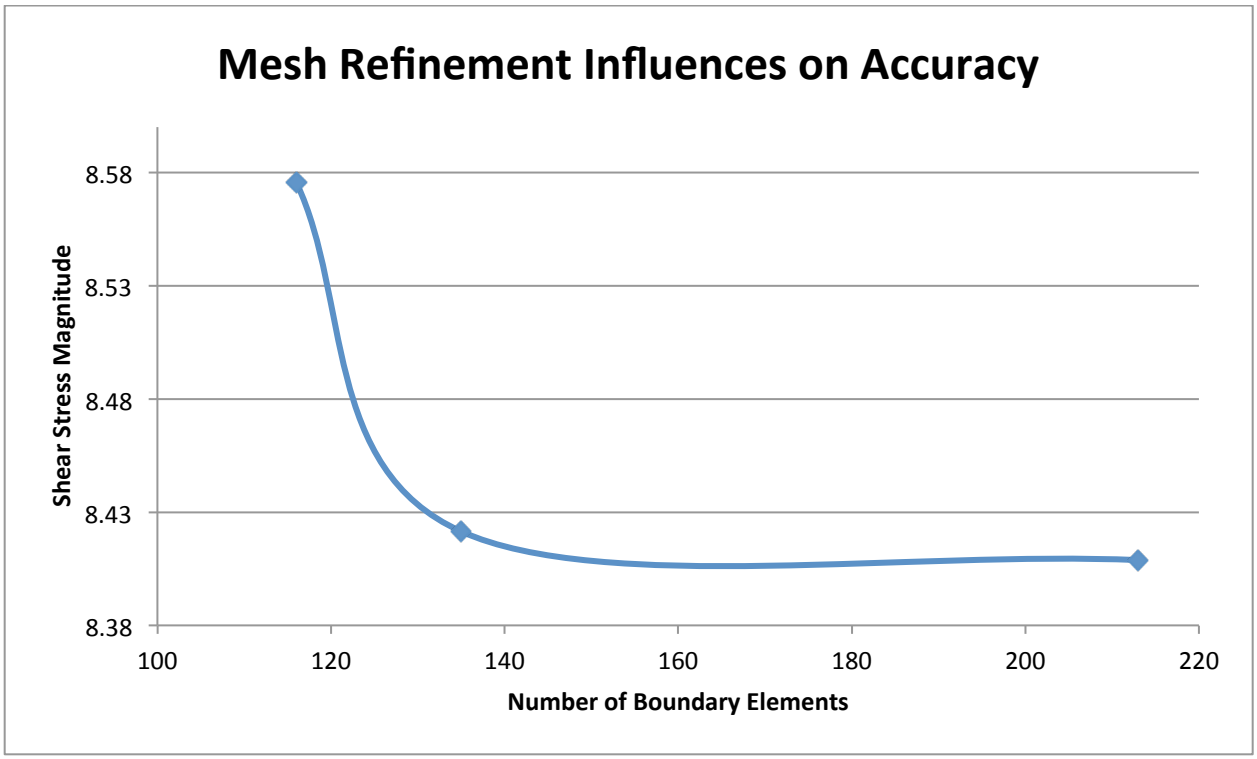

FIGURE 29: MESH REFINEMENT IMPROVES THE ACCURACY OF FEA EVALUATIONS.

It is necessary to choose an adequate mesh refinement for the desired accuracy of a model. This study assists in elucidating the importance of mesh refinement. By increasing the mesh quality surrounding the stent region, the shear stress magnitude was altered by 2%. Industry standards often desire mesh refinement accuracy less than 1%.

B.3 Symmetry of Navier-Stokes

There was symmetry in the shear stresses experienced by a single strut at each position. Figure 30 illustrates the labeling of each stent position to facilitate discussion, and Figure 31 is a plot of the shear stress experienced by each position along the strut.

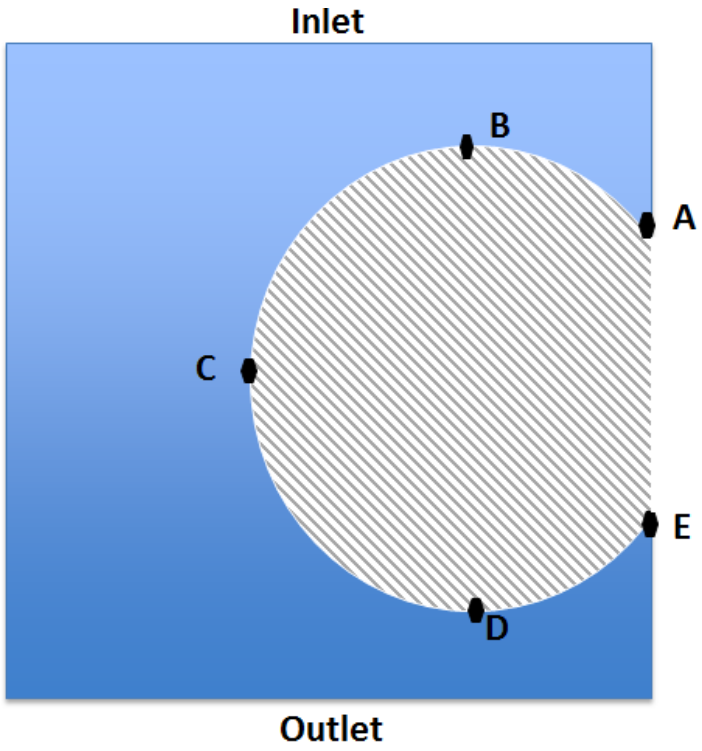

FIGURE 30: SCHEMATIC OF ANALYZED STENT POSITIONS IN COMSOL.

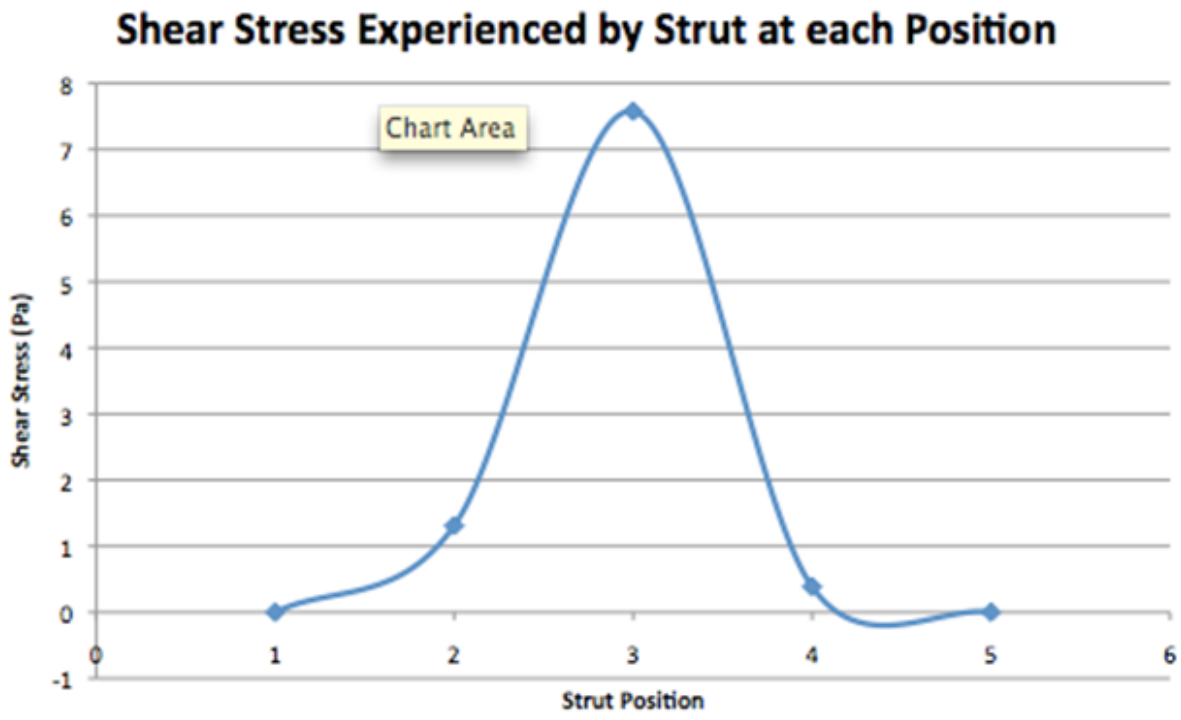

FIGURE 31: SHEAR STRESS EXPERIENCED BY THE STRUT VARIES BASED ON POSITION.

Using a full transient simulation, symmetry was noticed for the shear stress surrounding the strut. At positions A and E the shear stress was different by 0%. As positions B and D the shear stress magnitudes differed between 1.22% and 30%, with the stress at position B being consistently larger. Stokes flow always predicts symmetry. Navier-Stokes does not predict symmetry due to extra terms in the computations. Therefore, it is important to note, for design purposes, that flow rates give a symmetric wear pattern.

Appendix C: Complete Mathematical Derivation for Simple Mass Balance

This equation is a simplified version of the comprehensive degradation theory presented in Appendix X. The derivation utilizes experimental corrosion data and a simple mass balance on the stent strut geometry to predict the time required to reach a specified mass fraction of the material. This would be useful in determining the time required to degrade the stent at a fraction of the original mass, which would relate to changing mechanical properties with time.

$$\frac{dm}{dt} = -R_{exp}$$

The loss of mass with time is equal to the experimental corrosion rate.

$$\int dm = \int -R_{exp}\, dt$$

$where\ R_{exp} = Ae^{bt}$

$$Using\ u - substitution\ where\ u = bt\ and\ du = bdt\ yields\ the\ following:$$

$$m = -\frac{A}{b}\int e^{u} du$$

$$m = -\frac{A}{b}e^{u} + C$$

Solve for the integration constant, C, using the following initial condition:
m = m_o @ $t = 0$.

$$m_o = -\frac{A}{b}e^{0} + C$$

$$C = m_o + \frac{A}{b}$$

Plug the integration constant back into the equation and simplify.

$$m = -\frac{A}{b}e^{bt} + m_o + \frac{A}{b}$$

$$\frac{m}{m_o} = 1 + \frac{A}{b\, m_o}e^{bt}$$

Solve for time.

$$ln(e^{bt}) = \ln\left[\left(\frac{m}{m_o} - 1 - \frac{A}{bm_o}e^{bt}\right) * \left(-\frac{bm_o}{A}\right)\right]$$

$$t = \frac{1}{b}\ln\left[\left(\frac{m}{m_o} - 1 - \frac{A}{bm_o}e^{bt}\right) * \left(-\frac{bm_o}{A}\right)\right]$$

Appendix D: Comprehensive Rate Equation Theory

Design development requires significant resources: time, money, materials. Development of a stent design can require years of bench testing, in vitro and in vivo testing, to finally delve into clinical studies with the hopes of successfully being approved for the market. The motivation for developing a mathematical approximation to model material degradation was to expedite the initial evaluation process for possible material selection. A loss of material occurs due to corrosion and erosion. A comprehensive degradation equation could be determined to predict the lifetime of strut thickness by synthesizing experimental data and the theoretical shear stress values, which are known to effect erosion. A mathematical model would not take into account changes in the degradation rate due to cell adhesion or protein adsorption, but would create a baseline for material testing that requires fewer resources.

The experimental portion of this project addressed corrosion, but not degradation due to erosion. Material corrodes due to the chemistry of the solution, and is dependent on parameters such as ion concentration and pH. Erosion is due to fluid flow. The corrosion of the metal was evaluated in the experimental portion of this project, which did not address erosion. Erosion is not addressed in literature, but has been determined to be a function of shear stress. Discussing the effects of erosion is beyond the scope of this project, but would be a function of shear stress.

Figure 32 is a visual representation of the system used for deriving the corrosion rate equation. The image defines the initial variables used in the rate equation, where R_i is the initial distance from the centerline to the apex of the stent strut, defined as 1.36 mm.

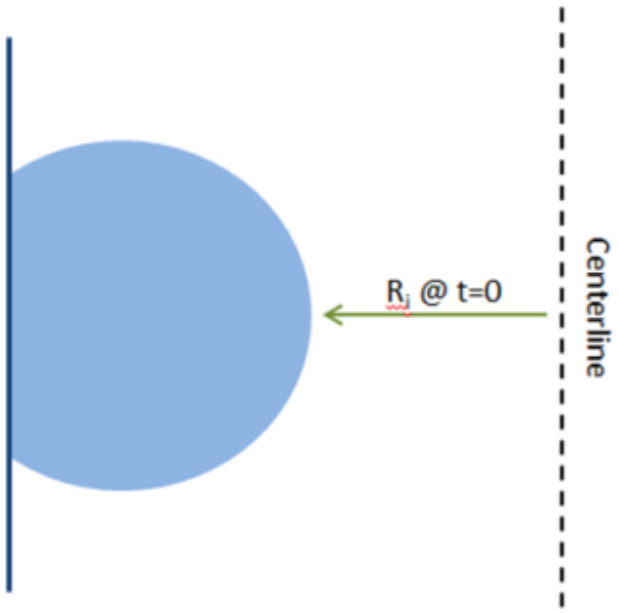

FIGURE 32: SCHEMATIC OF EVALUATED VESSEL AND STENT GEOMETRY.

For simplicity, a rectangular geometry was evaluated. When evaluated using one experimental corrosion equation, the equation yielded results off by a factor of 100 from the expected results. Therefore, we acknowledge there is error in this rate equation. However, this is useful for students continuing to pursue the project, and was therefore included in the report.

The equation to characterize the change in strut thickness over time was developed using a mass balance for a strut in the vessel, and is shown below.

$$\frac{\partial\delta(t)}{\partial(t)} = -\frac{(2R_i\delta(t) + \delta(t)^2)}{2(R_i + \delta(t))} * (R_c + R_e)$$

$$\begin{Bmatrix} Change\ in\ stent \\ strut\ thickness \\ with\ time \end{Bmatrix} = \begin{Bmatrix} function\ of\ distance\ from\ the\ centerline, \\ strut\ thickness, and\ degradation\ rate\ due \\ erosion\ and\ corrosion \end{Bmatrix}$$

Where R_c is the experimental corrosion rate and R_e is the erosion rate.
From Section X, the experimental corrosion rate was determined to be R_c = $1.0243e^{-0.015x}$. R_e is outside of the scope of this project and is not considered in this mathematical model.

$$\partial\delta(t) = -\frac{(2R_i\delta(t) + \delta(t)^2)}{2\big(R_i + \delta(t)\big)} * Ae^{bt}\partial(t)$$

$$\int \frac{2\big(R_i + \delta(t)\big)}{(2R_i\delta(t) + \delta(t)^2)}\partial\delta(t) = \int_0^t Ae^{bt}\,\partial(t)$$

Integral tables were used to evaluate the left side of the equation in parts, and u-substitution was used to integrate the right side of the equation

Evaluating the left side:

$$\int \frac{2\big(R_i + \delta(t)\big)}{(2R_i\delta(t) + \delta(t)^2)}\,\partial\delta(t)$$

Distribute and separate the integral.

Use the following integral conversions to solve.

$$\int_{\delta_0}^{x\delta_0} \frac{dx}{a^2 + b^2x^2} = \frac{1}{ab}\tan^{-1}\left(\frac{bx}{a}\right)$$

$$\int_{\delta_0}^{x\delta_0} \frac{xdx}{c + dx^2} = \frac{1}{2d}\ln\,(c + dx^2)$$

Where a =$\sqrt{2R_i}$, b = d = 1, c = $2R_i$, and $R_i = 1.36$ mm. X is the fraction of material desired to be left at the evaluated time.

Evaluating yields:

$$2R_i\left[\frac{1}{ab}\tan^{-1}\left(\frac{bx}{a}\right)\right]\Bigg|_{\delta_0}^{x\delta_0} + 2\left[\frac{1}{2d}\ln\,(c + bd)\right]\Bigg|_{\delta_0}^{x\delta_0}$$

Evaluating the right side of the equation yields:

$$\frac{A}{B}(1 - e^{Bt})$$

Combining both sides of the equation yields the full expression:

$$2R_i\left[\frac{1}{ab}\tan^{-1}\left(\frac{bx}{a}\right)\right]\Big|_{\delta_0}^{x\delta_0} + 2\left[\frac{1}{2d}\ln\left(c+bd\right)\right]\Big|_{\delta_0}^{x\delta_0} = \frac{A}{B}(1-e^{Bt})$$

Solving the expression for time yields:

$$t = \frac{1}{B}ln(-\frac{B}{A} * ((2R_i\left[\frac{1}{ab}\tan^{-1}\left(\frac{bx}{a}\right)\right]\Big|_{\delta_0}^{x\delta_0} + 2\left[\frac{1}{2d}\ln\left(c+bd\right)\right]\Big|_{\delta_0}^{x\delta_0}) + 1))$$

This is a comprehensive equation that evaluates the fraction of material remaining after a determined time. The fraction $x\delta_0$ allows for the evaluation of material remaining at any point in time. Ideally the equation would be used to evaluate several material options to elucidate possible material solutions based on the desired implant lifetime.

It is important to note that the corrosion rate is the primary contributor of degradation, and all other influential factors of degradation are secondary. Therefore, change in geometry and properties are dominated by corrosion. This is useful in design optimization and to allow for material optimization.

D.1 Further medical explanation of biomaterials and corrosion control

None of the predictions presented in the paper take into account biological factors such as protein adsorption and cell adhesion, which can also alter degradation rates of a material. Changes in velocity can alter the favorability of cell and molecular adhesion to the endothelial lining and the stent struts. It is optimal to promote the coating of the stent with endothelial cells and protein as quickly as possible. Coating the stent in cells and protein decreases the event of a device-associated infection, and adhesion of cells to the material creates a natural inhibitory event for corrosion of the material. In the case of magnesium-alloys, which are corroding too quickly, it is important to pursue the possibility of coating or altering the surface structure of the material to favor the adhesion of cells and proteins.

Atherosclerosis is most prominent in regions of disturbed flow and decreased shear stress. Shear stress is directly related to cell shape and function. Endothelial shear stress (ESS) is a possible predictor of atherosclerosis and restenosis due to stenting. Low or high ESS can develop atherosclerosis and outward remodeling. Changes in ESS due to a change in dynamic forces acting

on the vessel can later local hemodynamic factors. This can contribute to coronary obstruction development and progression.

EC bear a majority of the WSS. WSS is a component of the fictional forces that arise as a result of fluid flow. A change in WSS, not an absolute value, is responsible for changes in vascular homeostasis and remodeling. WSS ranges from 10-70 dynes/cm^2 in the arteries, based on location and geometric effects. The mean WSS in the arterial system is 15-20 dynes/cm^2. However, deviations from a baseline are more significant than a standard WSS magnitude. A decrease in WSS due to decreased fluid flow decrease the inner vessel diameter. This is considered negative remodeling and is characterized as hypertrohic vessel narrowing. Higher WSS works to maintain a constant release of chemicals by the EC to regulate SMC vasodilatation. EC dysfunction is attributed to decreases in WSS, which results in decreased EC regulation and increased SMC proliferation. These all contribute to the probability of a restenosis event. Altered hemodynamic forces contribute to endothelial dysfunction, and adversely modulate EC signaling and gene expression. Local flow disturbances result in decreased SS, which activates atherogenic genes. In contrast, sustained laminar flow and high SS are associated with down regulation of atherogenic genes. Therefore, it is necessary to understand the effects of flow on EC. This can help to researchers understand the development of vascular pathologies such as atherosclerosis, thrombosis, and in-stent restenosis that results from stent implants. Design optimization is possible by developing stent geometries that limit flow disturbance around the stent and promote healthy levels of WSS.

Critical WSS is defined in literature as less than 1.26 Pa [3]. The regions of cells surrounding the stent do not experience WSS values that meet this minimum. Therefore, these regions are at increased risk of restenosis, as well as decreased cellular viability. Possible methods to decrease the change in WSS pre and post-stent include altering the strut shape, as well as the ratio of strut width and height (W/H) [3]. Literature has shown that a rectangular strut results in the greatest drop in WSS compared to a baseline value, and a circular strut shape is more effective at maintaining the baseline WSS value. The effects of different struts shapes alter the magnitude of critical WSS experienced by a vessel. WSS distribution is variable in response to stent strut spacing. As the W/H ratio increases the flow reattaches to the wall, characteristic of a vessel without a stent. It is less optimal to use a stent with a W/H ratio less than 3, due to changes in flow that decrease WSS experienced by endothelial cells, and an increase in W/H from 3 to 6 results in increased WSS, closer to the WSS in an unstented vessel. Stenting, in all cases, decreases the WSS below the

optimal level for maintaining stress on the endothelial cells, and results in stagnation in regions surrounding the struts. However, changes in W/H are limited depending on the area of implant.